Summer 2013

Optimization of Solar Cell Arrays Using the Fibonacci Search Algorithm

Felicia Tyyan Farrow
Old Dominion University

OPTIMIZATION OF SOLAR CELL ARRAYS USING THE FIBONACCI SEARCH ALGORITHM

by

Felicia Tyyan Farrow
B.S May 2009, Old Dominion University

A Thesis Submitted to the Faculty of
Old Dominion University in Partial Fulfillment of the
Requirements for the Degree of

MASTER OF SCIENCE

ELECTRICAL AND COMPUTER ENGINEERING

OLD DOMINION UNIVERSITY
August 2013

Approved by:

Ravindra P. Joshi (Director)

Linda Vahala (Member)

Pawel Ambrozewicz (Member)

ABSTRACT

OPTIMIZATION OF SOLAR CELL ARRAYS USING THE FIBONACCI SEARCH ALGORITHM

Felicia Tyyan Farrow
Old Dominion University, 2013
Director: Dr. Ravindra P. Joshi

In our energy hungry world, there is a growing demand to develop creative mechanisms to extract, conserve, and use energy from different resources. The use of solar cells to extract and convert solar energy into electrical energy is a growing and popular field of study because solar energy is clean, free, and renewable. One limitation for photovoltaic (PV) or solar technology is its loss in efficiency and availability as a result of shading or partial shading. Shading or partial shading decreases the total capable output power that the PV system can produce because the array is receiving irradiation from the sun that is not uniform. This will result in reverse voltage, excess power to dissipate, and overheating to occur in the shaded or partially shaded PV cells. Over time, partial or total shading damages and shortens the life span of the costly PV panels.

A Fibonacci Search Algorithm has been proposed as a possible solution to alleviate this issue by searching and turning off shaded solar cell within a solar cell grid. This will reduce overheating and damage in the shaded cells from excess power dissipation.

The purpose of this thesis is to examine the implementation of the Fibonacci Search Algorithm using two techniques, Full and Quick Search, on modeled PV arrays. The computed and simulated results for both algorithms are presented and discussed.

ACKNOWLEDGEMENTS

I would like to express my sincere appreciation and gratitude to my advisor Dr. Ravindra P. Joshi for his guidance, feedback, ideas and support throughout this research project; and more importantly for him never giving up on his student. His help, patience, mentorship has made the completion of this thesis possible. It is an honor to work with him. I also wish to thank Dr. Linda L. Vahala and Dr. Pawel Ambrozewicz for taking the time out from their schedule and contributing their service and time to be part of my thesis committee.

I am very thankful for my family, my parents, James and Mona Farrow, my three sisters, Alicia, Kayla and Chanda Farrow, my grandparents, my aunts, my uncles, and cousins for believing in me, and their continuous support and encouragement as I pursued this endeavors. Above all, I am most thankful to My Creator, for blessing me to come this far.

I will like to dedicate this thesis to my late grandfather Roy E. Hinton. Despite being born a sharecropper in North Carolina and never completing and graduating from the 8th grade (because of the extra and much needed hand in the field); he has instilled in me the importance of life-long learning and going as far as I can go in my educational journey. Thanks Granddad for your humble spirit and committing your time to help me study during those afterschool hours and weekends. Thanks for prepping me for those tests and quizzes throughout elementary and middle school. Your fire still lives on....

--- Felicia Farrow

TABLE OF CONTENTS

LIST OF TABLES

LIST OF FIGURES

CHAPTER 1

INTRODUCTION

1.1 Introduction

Energy is essential to the growth and maturity of the world's social and economic development. Electrical power, heating, transportation, industrial activities, and cooking are the major sectors of energy consumption. The intensity and increasingly rapid growth of our agricultural, industrial and domestic activities result in the increasing demand for energy nationally and worldwide. The total demand for energy in the world from 1980s to 2006 increased from "7223 million tons of oil equivalent (Mtoe) to 11730 Mtoe"[6]. The increase in usage of our energy from coal, oil, natural gas, nuclear, etc., also amplifies greenhouse gas emissions in our atmosphere [2]. The rate of consumption of these resources versus the replenished rate is not sustainable. These resources are at risk of depletion. Therefore, to prevent rapid depletion and to reduce emission of greenhouse gases, alternative methodologies have been and are currently being developed. These alternative methodologies provide sustainable, cleaner, renewable, and innovative means of extracting energy for electrical power [6].

1.1.1 Renewable Energy/Power

Renewable energy is energy in which the sources are naturally occurring and replenished in the environment. These sources include sunlight, wind, water, biomass, geothermal and heat. Solar energy is extracted from the "heat and light of the sun" via various methods such as "solar heating, solar photovoltaic[s], solar thermal electricity,

and solar architecture" [25]. Wind power comes from the sun. The heat from the sun causes movement of air particles in the atmosphere and thus produces wind. Moreover, differences in air pressure cause the rapid movement of air from a pressure of high to low. The rotation of the Earth prevents the movement of air from a high to a low pressure from taking place right away; a phenomenon called the Coriolis Effect changes the direction of the air at the two hemispheres. In the northern hemisphere, the air deflects to the right, and in the southern hemisphere the air deflects to the left. Wind is the resultant of the air moving "around the high and low pressure areas". Energy from wind is harnessed into wind power via wind turbines [21]. Power extracted from turbines that is moving water from high to low potential is called hydropower [22]. Carbon, hydrogen, and oxygen based biomass is energy that comes from biological composition of living and decomposed organisms. Furthermore, this composition consists of dead plant matter, different species of living plant matter, garbage, and even municipal solid waste. This compost can be used as a direct energy source via combustion or the compost is converted to biofuel. Geothermal energy is energy extracted from the earth's heat using heat pumps. This heat comes from hot springs, hot water, hot rocks and molten rock or magna "found miles beneath the earth's surface[s]"[23,24].

As of 2007, 18% of the world's energy comes from renewable energy and approximately 80% of this renewable energy is from biomass in developing countries. 17.6% of the 18% renewable energy generated is for electrical production, and hydropower makes up 90.3% of that electrical power from the same 17.6% mention previously. The sun is the source of all renewable resources except for geothermal and tidal [5,21].

1.2 Overview of Thesis Research Objectives

In our energy hungry world, there is a continuous demand in developing creative ways to extract, conserve, and use energy from different resources. The use of solar cells to extract and convert solar energy into electrical energy is a growing and popular field of study because solar energy is clean, free, and renewable. One of the major setbacks of photovoltaic (PV) or solar technology is its efficiency and availability. Solar energy availability is limited during the night, during rainy and severe weather conditions, and in some cases winter seasons. Moreover, in residential, commercial, and industrial applications, as the sun moves across the sky the possibility of shade on photovoltaic cells from nearby trees, buildings and clouds impact and limit the total power the photovoltaic system produce to a potential utility grid or residential home. In addition, shading on a PV cell results in reverse voltage of the affected cell and in return damages and shortens the life span of the costly PV cell [26]. This too, affects the efficiency of the system. Therefore, research is being done on possible methods and ways to mitigate the effect shading has on the cell. This thesis objective focuses on examining three different size PV arrays and tracking the maximum power generated from individual cells in a PV array and turning off potential cells that are outputting low power when compared to maximum power.

Moreover, the optimization techniques used in computing the maximum power uses two algorithms, Fibonacci Full Search Algorithm and Fibonacci Quick Search. The aim of this thesis is to analyze and compare the results of the two algorithms.

Chapter 2 provides a background literature review of solar energy and photovoltaic technology. Chapter 3 details optimization techniques, Fibonacci numbers

and sequence, Fibonacci Search Method, and the Fibonacci Full and Quick Search Algorithms. Two examples are provided in that chapter. Chapter 4 gives the output power and voltage results of the two algorithms from different PV arrays models and provides discussions. Finally, Chapter 5 concludes with a summary of the results, followed by limitations and potential future research study in this area.

CHAPTER 2

BACKGROUND AND LITERATURE REVIEW

2.1 Introduction

This chapter provides a background and literature review concerning research conducted on solar energy, the photovoltaic effect, and solar technology including photovoltaic technology.

2.2 Solar Power

Petawatts of solar radiation comes to earth every day; 70% is "absorbed by clouds, oceans, and land masses" while the remaining "30% is reflected back to space" [26]. The process in which this solar radiation and energy is converted into electricity is called solar power technology. Solar power technology is divided into two main categories depending on the methodology in which the solar energy is "captured, converted, and distributed." There is a direct or active method involving photovoltaic panels and there is an indirect or passive method using concentrated solar technology [25].

2.2.1 Indirect Solar Power (Concentrated Solar Power)

Concentrated Solar Power (CSP) "concentrates" the direct sunrays normal to a surface plate collector or receiver [13]. CSP technology "absorbs and converts" the solar energy into heat via steam turbines, Stirling engines, or gas turbines to produce electricity. Heat transfer fluid (HTF) "flow[s] through the collector[s]" and transports the

heat to the stream turbines and engines. HTF such as water, air, oil, or molten salt connects "the solar collectors to the power generation system"[5]. The type of HTF depends on the electrical generation system i.e., the type of turbine or engine used in a CSP system. CSP falls into two main classifications: "Stationary, Non-Concentrating Collectors (SNCC)" and "sun-tracking concentrating collectors (STCC)"[5]. STCCs are more efficient than SNCC and moves with the sun during the course of the day to ensure that the "maximum solar flux" is directed on the collector [13]. SNCCs utilize a designated area to assimilate the sun's radiation and are less costly than STCC. According to Barlev et al. STCC is further broken down into four main subcategories: (1) Linear Fresnel Reflectors (LFR), (2) Parabolic Trough Collectors (PTC), (3) Parabolic Dish Collectors (PDC) (also known as Dish-Stirling), and (4) Heliostat Field Collectors (HFC), also known as a Solar Tower. Table 2.1 gives a brief description of the four types of STCC [5].

Table 2.1: Four types of STCC [5]

Concentrated Solar System	Solar System Character-istics	Efficiency	Functionin-g Temperatu-re Range (deg Celsius)	Price	Sun Concentration Ratio (Sun)	Age of Technolog-y/ Maturity Level	One or Two Tracking Axis
PTC	Reflective aluminum acrylic parabolic sheets Metal Pipe Linear receiver with HTC	Low	50-400	Low Cost	15-25	Very mature	One-axis

Linear Fresnel	Flat mirror arrays directed on tower and mounted LRF	Low	50-300	Very High Cost	Oct-40	Mature	One-Axis
Solar Tower	Centered tower surrounded by large heliostat field Receiver using water as the HTC Capable of continuous thermal storage	High	300-2000	High Cost	150-1500	Most recent	Two-axis
Dish Stirling	Stirling engine receiver Reflective parabolic dish Operates with/out HTC	High	150-1500	Very High Cost	100-1000	Recent	Two Axis

LFRs and PTCs are similar in concept. LFRs consist of elastic, flat mirrors (reflectors) aligned in an array configuration. These mirrors focus the sun's beams onto linear receivers that are attached on top of a tower that is 10 to 15 meters in height within an array of mirrors shown in Figure 2.1. Each mirror is positioned on top of a "two axis tracking device" [5].

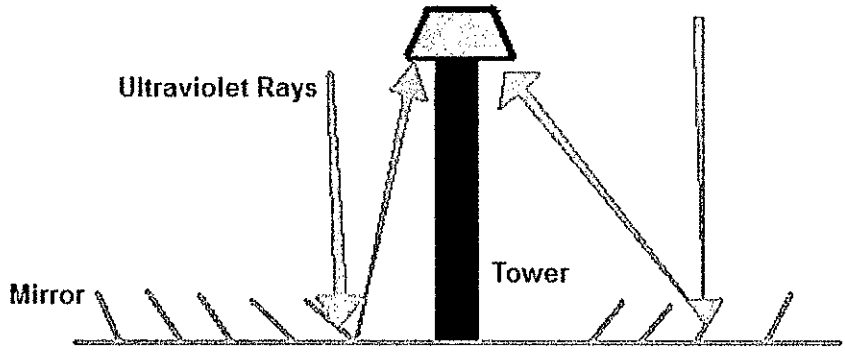

Figure 2.1: Linear Fresnel Reflector Diagram [5].

As shown in Figure 2.2, PTC design is composed of tracking mechanisms, pedestals, receivers, and reflective sheets made up of silvered acrylic; these sheets are parabolic in shape and are arranged in "series to form long troughs" [5].

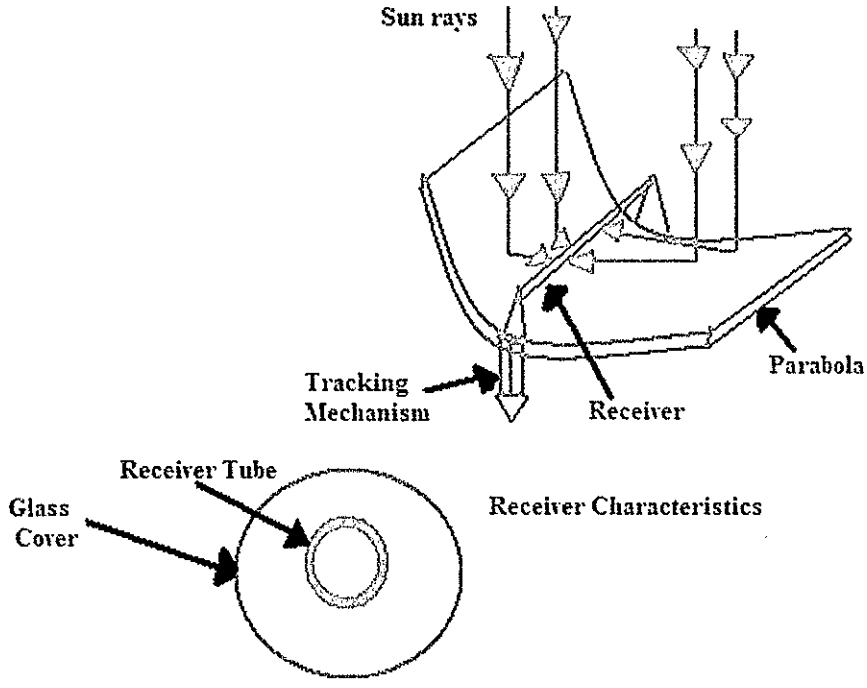

Figure 2.2: Parabolic Trough Collector [5].

Serving as tracking mechanism, pedestals on the ground support the parabolic troughs on opposite ends of the trough and each of these parabolic troughs exhibits a focal line (see Figure 2.2) where a black metal pipe receiver is placed. The tracking devices ensure that normal/incident sun's rays are hitting the surface at an angle that is parallel to the reflective parabolic surface and concentrated on the receiver during the entire day. Thermal energy is gathered and carried in the receiver by HTF to "electric[al] generation systems" such as turbines, boilers, and/or storage systems. To reduce convectional heat loss, the receiver is enclosed in a glass pipe [5].

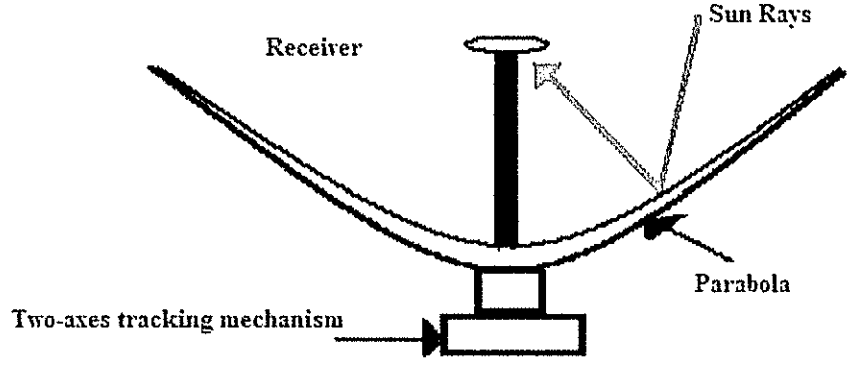

Figure 2.3: Parabolic Dish Collector [5].

Shown in Figure 2.3, the parabolic collectors of PDC are mounted on two axes tracking devices; these devices follow the sun throughout the course of the day to ensure that the sun light converge to the parabolic focal point of the collector where the receiver is position to absorbed the heat of the solar radiation. Two different approaches are used to extract electricity from the heat collected in the receiver. Similar to the other CSP types, one approach uses HTF in the receivers that transport the thermal energy to a "central electricity generation system."[5] The alternative approach utilizes heat engines

that are placed close to or at the focal point of each collector. The heat engines take the thermal energy collected from the receiver and convert that energy to mechanical energy. The mechanical energy is then delivered to alternators that produce electricity. "A heat waste exhaust system" is built in to prevent overheating and to remove surplus heat from the heat engines. In addition, the use of heat engines also mandates control systems to maximize the operation of the heat engine to the "incoming solar flux" [5].

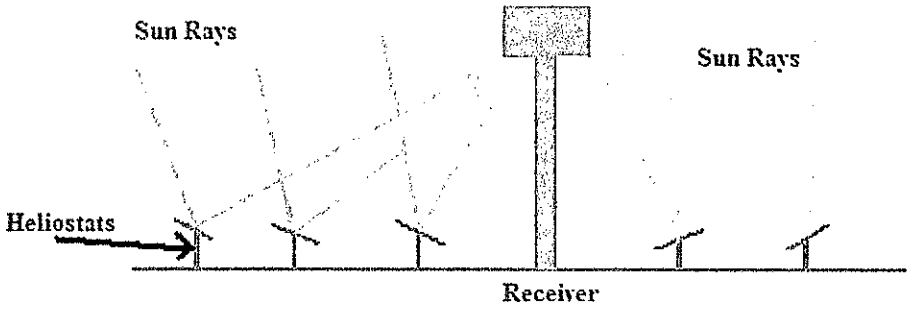

Figure 2.4: Heliostat Field Collectors [5].

The components of a HFC's system shown in Figure 2.4 include central receiver unit, tower, flat slightly concave mirrors called heliostats with surface area of 50 to 150 m, and two-axis tracking bases. The system set-up involves a cluster of heliostats arrays individually mounted on a two-axis tracking base. The heliostats circumvent a receiver mounted on top of a tall tower that ranges from 75-150m in height [9]. The receivers are purposely placed on tall towers to optimize the arrangement in which the heliostats can be placed from each other in order to minimize and avoid shading. Heliostats are uniquely arranged such that the reflected sunrays are incident to the central receiver. Just like the other CSP types, HTF flows through the receiver taking the absorbed thermal

energy to a power station such as steam or turbine generators to generate and store electrical power [6].

CSP plants exhibit the greatest "potential in the sun belt" regions of the earth [13]; they are limited to certain geographical locations because of their size and configuration [9]. These limited regions are usually large remote flat desert terrains with minimal cloud coverage, and thus receive significant amounts of sunlight. Therefore, these features are desert regions. Solar One, located in Nevada, has the world's largest CSP commercial plant facility with power capable of exceeding 200 MW [9].

2.2.2. Direct Solar Power (Photovoltaic)

Photovoltaic (PV) technology is the direct conversion and production of electricity from sunlight without using thermodynamic process such as heat/steam engine (or any other process) to transform the sunlight to electricity [5]. This technology utilizes the characteristics of semiconductors to "directly convert solar radiation into electricity" [7]. Silicon crystalline structures and thin film structures are the two broad categories for PV technology that have emerged over the years. PV system consists of individual cells called wafers prepared from thin films or crystalline silicon that react to sunlight; and once exposed to solar radiation, "a small direct current is produced"[7]. Groups of these cells are arranged into a large cluster grid called modules. Collectively, these modules output electricity without emitting noise and harmful pollutants in the atmosphere. PV systems as a whole include solar cell modules, and additional electrical components such as inverters, and charge controllers. Those electrical components manage and direct the

electricity to appropriate DC loads or convert the DC power to "AC power for use by AC loads." [2, 7].

2.3 The Photovoltaic Effect

2.3.1 History

In 1839, physicist Alexander-Edmund Becquerel is credited with igniting the start of PV technology via his discovery of the photoelectric effect which involves finding out that "electrical currents [arising] from certain [types of] light induce chemical reactions" [8,10]. During his experiments, he placed a pair of electrodes in a conductive solution, exposed them to light, and noted that between the two electrodes electron emissions increased. Table 2.2 gives a summary timeline of PV technology advancements. Decades later, other scientists started examining the photoelectric effect in selenium and noted comparable results. Devices that accurately calculate the "exposure time of photographic material[s] or film[s]" based on the illumination of the materials or films' surfaces arose in 1870s [10]. In 1873, Willoughby Smith, a British engineer, conducted various experiments concerning materials for underwater telegraph cables and noticed selenium sensitivity to light. He observed that the resistivity of selenium exhibits an inverse proportional relationship to the intensity of light" [10]. His experiments and notes concerning selenium photoconductivity greatly contribute to the development of "selenium cells in utilizing solar energy" [7]. Next in 1883, American Inventor Charles Fritts created the first "PV cells" via coating selenium wafer with "transparent gold film," generating a small current with a 1% maximum efficiency [7]. Since selenium wafer exhibited low efficiency and because of the rarity of the element selenium, fabricating

these wafers and power production during this time was "impractical" and expensive. The development of the first solid-state device in 1940 embarked the production of the 6% silicon solid cell industry in the 1950 [10]. The contributors to the PV cell 6% efficiency were Bell researchers, Calvin Fuller and Gordon Pearson. Examining the potential use of incorporating silicon into rectifiers and transistors, Pearson and Fuller found that doping rectifiers and transistors with "certain impurities" enhanced their electrical properties [7].

Table 2: Timeline showing the advancement of PV technology [10].

Significant Dates in the History of Photovoltaic Solar Energy Technology	
Scientist and Innovation	Year
Becquerel discovers the photovoltaic effect	1839
Adams and Day noticed photovoltaic effect in selenium	1876
Planck claims the quantum nature of light	1900
Wilson proposes Quantum theory of solids	1930
Mott and Schottky develop the theory of solid-state rectifier (diode)	1940
Bardeen, Brattain, and Shockley invent the transistor	1949
Charpin, Fuller, and Pearson announce 6% efficient silicon solar cell	1954
Reynolds et al. highlight solar cell based on cadmium sulphide	1954
First use of solar cells on an orbiting satellite Vanguard 1	1958

During the mid to late 1960s, because of the space race, spacecraft and satellite technologies began to incorporate PV technology via the use of solar energy to power satellites in space. Toward the late 1960s and early 1970s, PV technology was beginning to be used by industries and the residential sectors [7,8].

2.3.2 PV Theory

Solar energy is electromagnetic radiation, and is distinguishable according to wavelength via the electromagnetic spectrum. Each type of electromagnetic radiation exhibits its own "photons of electromagnetic energy", a "photon is a unit of electromagnetic radiation"[2]. These photons can be expressed as a wave $\lambda=v/f$ and as a particle with its energy equation $E= hf$. Recall from chemistry, electrons want to occupy the lowest states [1,2]. Therefore, when an electron goes to the lower orbital, it releases photon of energy [7] and the quantity is proportional to the difference in orbital energies of the electron. When a photon of energy penetrates another atom, the atom takes in this photon of energy, resulting in electrons jumping to a higher energy state or orbital. However, for the electron to move to a higher energy state, the absorbing photon energy has to be equal to the difference in the electron energy orbital levels also called the band gap energy. Also, recall that in semiconductor materials, electrons exhibit weak bonds in the valance band of their respective atoms. These weak bonds are broken once energy that surpasses the band gap energy is absorbed in the valance band. This results in the electrons, now with enough energy to migrate to the conduction band; the flow of electrons in the conduction band generates a dc current in the material [2].

When sunlight illuminates a given semiconductor material (used in PV cells), electrons flowing within the material absorb or reflect the solar photons, or the photons pass through the atoms that make up the material. If the absorbed photons are equal to the difference in the electrons current orbital levels and the next higher orbital levels, the electrons jump to the next orbital or leave the atom. The electrons that leave the atom conduct an electric current. This phenomenon is called the photovoltaic effect [2].

PV cells are thin flat wafers with p-n junctions. When p-n junctions are exposed to light, electrons in the upper n-type layer of the device absorb the light photons causing the excited electrons to jump states to the conduction band. As these electrons jump states, they leave a positively charge hole in its place. The movement of holes and electrons produces an electric field in the p-n junction [2]. This electric field prevents the immediate recombining of electrons and holes. Because of the repulsion and attraction forces, electrons move away from the p-type layer to the surface of the material and the holes migrate from the n-type layer towards the bottom layer. The build-up of negative charge electrons in the n-type region and holes in the p-type region produces an electric potential "between the top and bottom surface" [7].

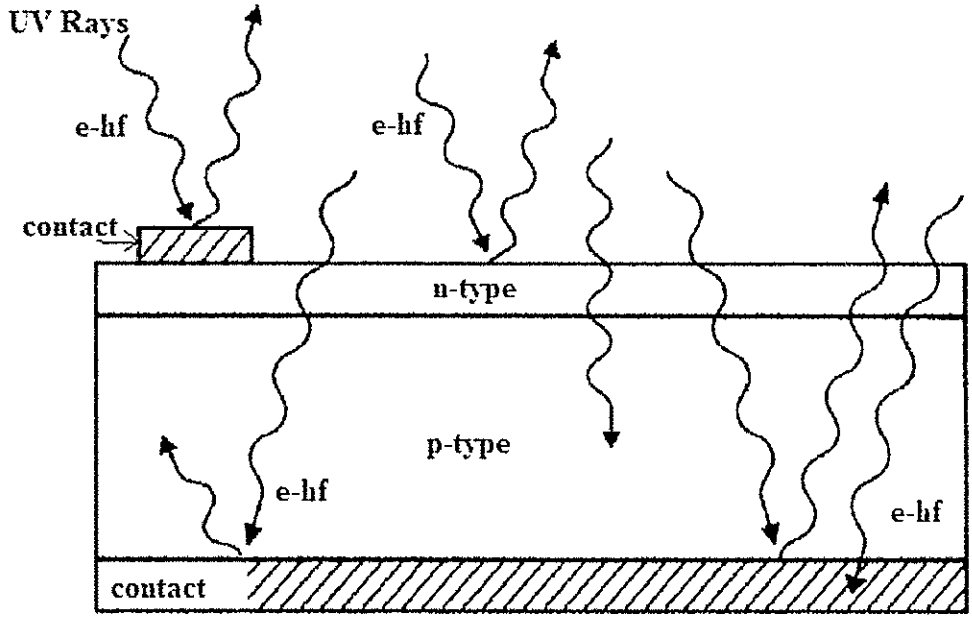

Figure 2.5: Diagram of Photovoltaic Effect (10).

As shown in Figure 2.5, the p-n junction has two "selective metal contacts" protruding from the conduction band. Electrons flow out of one metal contact terminal in an external closed loop circuit. These external circuits involve circuitry wired to conduct electricity that can power spinning ceiling fans, sewing machine, or light bulb. Electrons moving through these external circuits lose energy as they perform work and soon return to the valance band in the semiconductor of the solar cell through the second selective contacts [2].

2.4 Solar Cells/Photovoltaic Arrays

2.4.1 Material Composition

Silicon is the most commonly used element in PV material because of its abundance (second next to oxygen), efficiency (compared to other metals), low material costs, environmental friendly, stability, and "a near optimum energy band-gap"[2]. Silicon does not occur purely on its own in nature; but it occurs with oxygen resulting in oxides and silicates. Therefore, silicon is extracted from the "high purity quartzite SiO2 ore"[2]. Twenty-six percent of the earth's crust is composed up of silica or silicates and other elements such as oxygen, magnesium and aluminum. At 25 degrees Celsius, Si exhibits a band-gap of 1.12 electron volts (eV). The crystalline structures of the fast growing epitaxial films and poly-silicon deposition as well as the "slow growing faces of SI" are {111}. Amorphous silicon is made from the vapor deposition when temperatures drops below 500° C and the material reverts back to crystallized silicon when it is "reheated" at temperatures surpassing 500° C. [2] Elements such as boron and phosphorous are impurities purposely added to the silicon semiconductor "during

processing to control the properties and doping levels of silicon"[2]. Doping silicon with impurities results in a brittle semiconductor; therefore, additional procedures such as sawing and grinding are done to shape silicon for PV use. Silicon's absorption and transmission spectral wavelength characteristics range from 0.4-1.5 μm. These characteristics influence the quality of the cell. The element used in the PV cells contacts is Ag; however, because of rising gold prices, this element is becoming a "limiting material" for PV technology [2].

2.4.2 Manufacturing /Technology

Silicon crystalline structures are the first generation of PV solar cells. Research in improving PV capability and efficiency spurred the development of different variants in the technology such as mono-crystalline, emitter wrap through (EWT), thin film technology, and compound semiconductors. This thesis is concerned with silicon crystalline structures and thin film technology.

Mono-Crystalline (MC) cells makes up approximately 80% of PV market because of it efficiency and cost. It utilizes a "crystalline Si p-n junction." During manufacturing, implementing the Czochralski method, "a single crystal ingot" is cultivated with a diameter ranges from 10-15 cm [10]. Precise machinery cuts the ingot into individual wafers that are 0.3 mm thick and each wafer exhibits properties of 35mA per cm^2 and 0.55V "at full illumination." Properties of silicon material inhibit further enhancement in the cell efficiency. These properties involve the reduction of energy emitted by photons at longer wavelengths, and at longer wavelengths, thermal energy dissipates within the PV cell resulting in reduction of its efficiency as the cell heats up[10]. MC cells have a

recorded maximum efficiency under standard test conditions of 24.7%. Efficiency is this low because of losses due to the cell's metal contacts, resistance, and reflection of solar radiation. It is important to note that efficiency of the module is lower than the individual cells.

Created by Evergreen Solar Company, Poly-Crystalline (PC) cells involve the technique of first "melting and solidifying" the silicon material, then holding the cooled crystals in an unchanged position allowing a rectangular MC ingot to grow [10]. Once that process is complete, machinery then cuts ingot into blocks and further slices it into a thin wafer. An alternative to the last two steps is via "cultivating wafer thin ribbons of poly-crystalline silicon" [9]. This PC technique was developed to reduce "flaws in metal contamination and crystal structure" [2,10]. Enhancement in the PV cell design led to the development of emitter wrap-through (EWT). An EWT design cell does not have a metal contact on the front or top of the cell but rather the contacts are located on the back. Moreover, lasers penetrate holes in the cell that joins the n-type contact located at the back of the cell to the "opposite side emitter "[2,10]. With the absence of metal contacts and lines for the contacts, the entire upper surface area of the cell takes in more solar light and the cell's efficiency increases 15-20% [2,10].

With thin film technology, sputtering tool place thin sheets 10 μm of "certain material" on stainless steel or glass substrates. These thin sheets have lower manufacturing costs because the materials are cheaper and the "high throughput deposition process" [2, 10]. Unfortunately, these thin sheets have less material area to absorb solar energy therefore, the efficiency in comparison to crystalline cells are lower. Currently, there are four main types of thin films cells: (1) cadmium telluride (CdTe)

hetero-junction cells, (2) amorphous multiple-junction structure silicon cell, (3) copper indium di-selenide (CuInSe2)/ copper indium gallium di-selenide (CIS) hetero-junction cell, (4) and thin poly-crystalline silicon on a low cost substrate [2,10] .

CdTe modules also known as cadmium telluride/cadmium sulphide have efficiencies greater than 9% and the cells efficiencies are greater than 15%. It also has high efficiencies during the manufacturing process. CdTe exhibits an optimum bandgap for solar cell because the material has "a high direct absorption coefficient" [2]. This type of thin film is "easier to deposit" and is "more apt for large scale production" for Ohio's 40 MW CdTe plant; Abu Dhabi has 5MW capability, and Germany has 10MW. CdTe is toxic to the environment and this issue has yet to be resolved. First Solar has developed a program to recycle decommissioned thin film CdTe cells [2,10].

Amorphous Silicon PV cells are based upon silicon atoms randomly positioned in a crystalline atom. This phenomenon has an impact on the material's electrical properties and the band-gap. The band-gap energy increases to 1.7eV, 0.6eV higher than the crystalline silicon PV cells. This increase in band-gap increases the cells' ability to take in "the visible part of the solar spectrum more strongly than the infrared portion of the spectrum" [10]. Of the four types of thin films technologies listed, amorphous silicon is the oldest. The deviations from amorphous silicon technology is attributed to the flexibility in the use of glass or stainless steel substrates and the junctions being tandem, double or triple junctions [10].

The elements composed in the CuInSe2/CIS thin film material are located in groups I, III, and VI of the periodic table. Elements in those groups exhibit "high optical absorption coefficients" [10]. The use of selenium in the CuInSe2/CIS thin films allows

for improvements in the semiconductors' uniformity and reduces the amount of recombination spots in the film. With fewer recombination spots, both quantum and conversion efficiency increases. The drawback of CuInSe2/CIS thin films is the rarity and possible future shortage of indium for the element is used in the manufacturing of flat screen displays of TVs, computers, and cell phones. Another drawback is the degradation that takes place within both modules when they are exposed to extreme heat or damp conditions. The degradation in the junction affects the "transport properties and minority carrier transport" characteristics of the cell and this in turn affects the ability of the cell to absorb solar radiation. Therefore, these cells are coated to prevent degradation [10].

2.4.3 Energy Storage

Solar energy is not available 24 hours and the available fluctuates according to weather, season, and time of day. The availability throughout the day affects the electrical loads; therefore, to prevent the electrical overload and to maintain balance, an energy storage element is installed in the PV power supply system. One such storage element involves capacitors collecting energy in the electric field between the capacitor plates. Capacitors store energy for range duration of microseconds to 10 nano-seconds. Electrochemical batteries are the most popular electrical storage elements used in PV systems [4]. Electrochemical batteries transform the "electrical energy into chemical energy" via converters and a chemical compound stores the energy. When extracting energy from the battery, or when the battery is discharging, the process is reverse. These steps are further shown in Figure 2.6 [2].

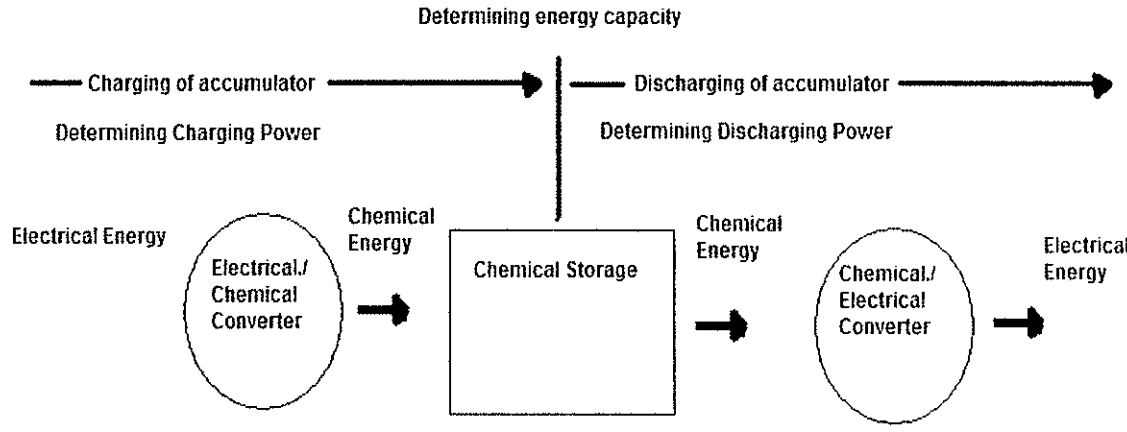

Figure 2.6: Electrochemical Storage Diagram [2].

2.4.4 Circuitry, Setup and Topologies of Arrays

The basic circuit model of a PV cell is shown in Figure 2.7 and this model consists of three elements, photocurrent source I_{pc} in parallel to diode D, and a series resistor R_S in series with the diode. The series resistance models the "internal resistance" and "ohmic losses" of the cell. V represents the voltage of the cell [3,11].

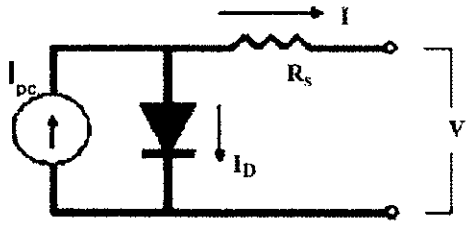

Figure 2.7: Schematic Diagram 1 of PV Cell Equivalent Circuit [10, 11].

The current going across the diode is given by the Shockley equation as follows:

$$I_D = I_S\left(e^{\frac{q(V+R_S I)}{QKT}} - 1\right), \qquad \text{(Eq. 2-1)}$$

where I is the current of a single PV cell, I_S is the diode's reverse saturation current, q is the charge of an electron ($1.61.6x10^{-16}C$), K is Boltzmann constant ($1.6x10^{-23}$Joules/ Kelvin), Q is the ideality and shape factor of the cell taking into account the imperfection of the cell, and T is the absolute temperature in Kelvin [10,11]. The saturation current I_s is defined as:

$$I_s = ZT^3 e^{(\frac{qE_g}{QKT})}. \quad \text{(Eq. 2-2)}$$

In this above equation, the variable Z is the diffusion constant of the diode with respect to temperature and E_g is the band gap [11]. Temperature affects the diode saturation current [10].

The I/V equation for the circuit shown in figure 2.7 is:

$$I = I_{pc} - I_s\left(e^{\frac{qV}{KT}} - 1\right), \quad \text{(Eq. 2-3)}$$

and,

$$V = IR_s\frac{P_s}{P_p}\ln(1 + \frac{P_p I_{ph} - I}{P_p I}), \quad \text{(Eq. 2-4)}$$

where P_s stands for the cells in series and P_p represents the cells in parallel [10].

Another basic circuit model of a PV cell is shown in Figure 2.8, with an added shunt resistor R_{Sh} in parallel diode and a resistor R_s is in series with the shunt resistor [3].

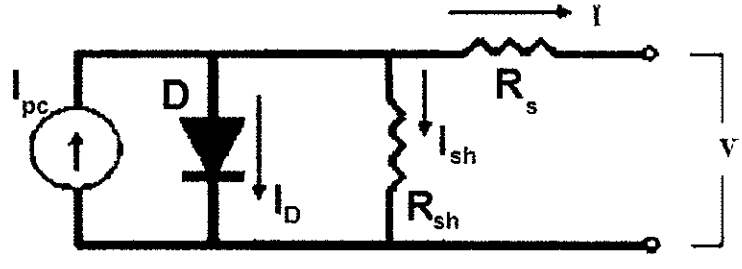

Figure 2.8: Schematic Diagram 2 of PV Cell Equivalent Circuit [3].

The shunt resistance models the "losses due to diode leakage currents" [3] and "leakage at the junction" [11]. Shunt resistor and series resistor collectively affect the voltage/current properties of the cell [3].

For the circuit shown in Figure 2.8, the I/V equation is:

$$I = I_{pc} - I_s - I_D \quad \text{(A)}, \tag{Eq. 2-5}$$

and,

$$I = I_{pc} - I_s \left(e^{\frac{q(V+R_S I)}{QKT}} - 1 \right) - \frac{V+R_S I}{R_s}. \tag{Eq. 2-6}$$

Irradiation and temperature affect I_{pc} and this relationship is shown in the equation below:

$$I_{pc} = \frac{W}{1000}(I_{sc} + C_T(T - 298)), \tag{Eq. 2-7}$$

where W is the irradiation, C_T is the temperature coefficient, and I_{sc} is the short circuit current [11]. V_{oc} *and* I_{sc} are the open circuit voltage and short circuit current of PV cell and "these values changes proportionally to the cell irradiance" [10]. I_{sc} is found by setting $I_{sc} = I_{pc}$ and cell voltage V = 0V [10].

A PV module, shown in Figure 2.9, consists of an array of PV cells; and connecting the cells in parallel increases the current and connecting the cells in series increases the voltage [11].

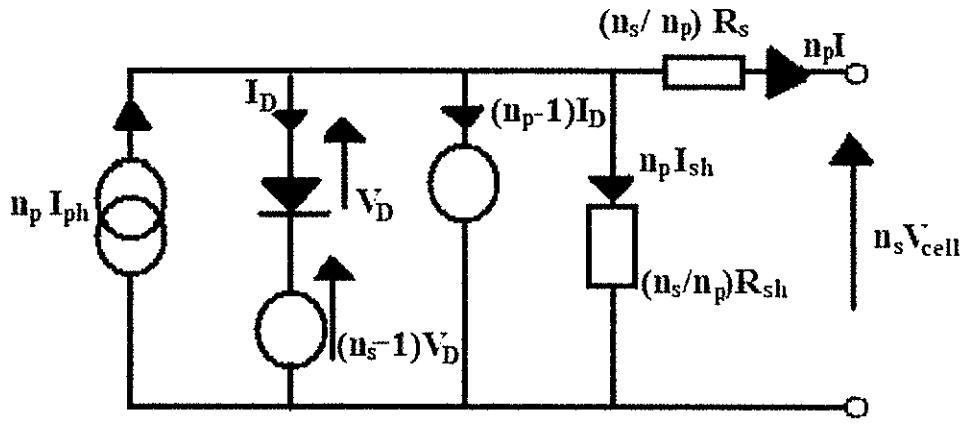

Figure 2.9: Schematic Diagram of PV Module Equivalent Circuit [11].

The PV module current equation is defined:

$$I_{array} = P_p I_{pc} - P_p I_s \left\{ exp\left(\frac{q}{P_s QRT}(V_{array} + I_{array} R_s \frac{P_s}{P_p}\right) - 1 \right\} - \frac{V_{array}\frac{P_s}{P_p} + R_s I_{array}}{R_{sh}}$$

(Eq. 2-8)

As the temperature increases the output power decreases, considering everything else remains constant. Figure 2.10 shows this relationship in its PV cell (a) Current (I) versus Voltage (U) and (b) Power(W) versus Voltage(U) graph at different temperatures. Figure 2.11 shows a) I versus U (b) W versus U relationship of a PV cell at different light intensities. Figure 2.11 highlights the relationship between the output power and light intensity up to a certain value, the value in which the power is at its maximum is called the maximum power point (MPP) [12].

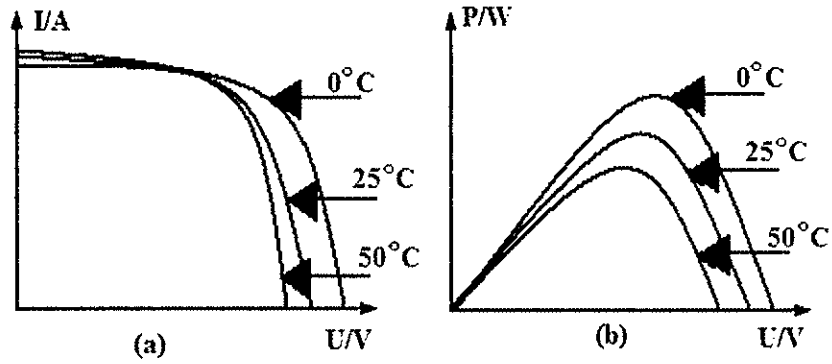

Fig. 2.10: PV Cells Relationship at Various Temperatures (a) I versus U and (b) W versus U [12].

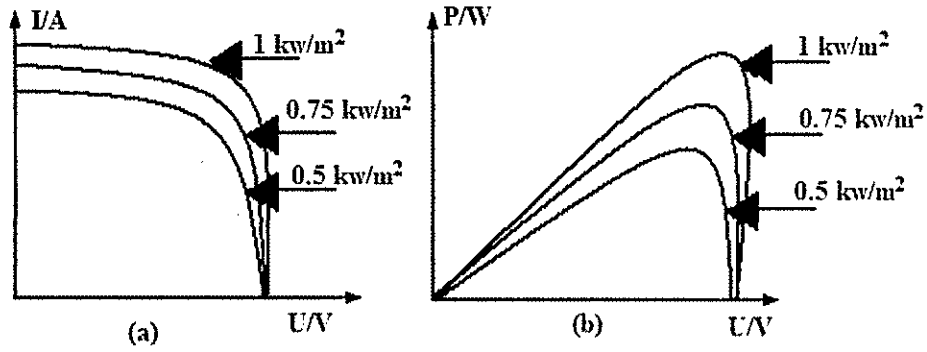

Fig. 2.11: PV Cells Relationship at Various Light Intensities a) I versus U (b) W versus U [12].

Chaar et al. further define that maximum power (MP) point (MPP) is the value in which the product of the current I_{mp} and the voltage V_{mp} is at its maximum [10]. This is found by taking the derivative of the product of current and voltage equations provided in equations 3 and 4, $\frac{d(VxI)}{dt}$ [9]. The fill factor, FF, of a PV cell characterizes the quality of the cell via the "junction quality and series resistance" where a FF value near one denotes high PV module quality [10]. The fill factor can be expressed in terms of the short circuit current I_{sc} and open circuit voltage V_{oc} as:

$$FF = \frac{V_{mp} \, x \, I_{mp}}{V_{oc} \, x \, I_{sc}} . \qquad \text{(Eq. 2-8)}$$

The power conversion efficiency μ is defined as $\mu = \frac{FF\ x\ V_{oc}\ x\ I_{sc}}{P_{in}}$, where P_{in} is the "incident power depending on the light spectrum incident upon the PV cell [11,12].

2.4.5 Limitations/ Efficiency Usage

The limitation of single-junction cells, affecting the efficiency depends on the photons energy and the cell's band-gap. When the photon energy is "below the band-gap," the cell is unable to absorb the energy and the energy is lost. On the contrary, when the photon energy succeeds the band-gap energy, the excess energy dissipates out as heat [2].

2.5 Photovoltaic Power Systems/ Photovoltaic System

There are two main types of PV systems: off grid and on grid. Off grid systems are applied to residential, consumer products (for calculator, watches, and garden lighten), commercial (for medical refrigeration, and DC water pumping), in village power AC such as micro grid, and in space applications. On grid systems applications include residential (storage and no storage), commercial (roof, carport and ground), and central and distributed utility systems. On grid systems have lower installation costs vices off grid and are cheaper to maintain. Moreover, on grid "operates more efficiently" than off grid systems [2].

2.5.1 Topologies

DC off grid PV systems shown in Figure 2.12 "directly use the DC energy" from PV modules "to supply power to DC loads" [2].

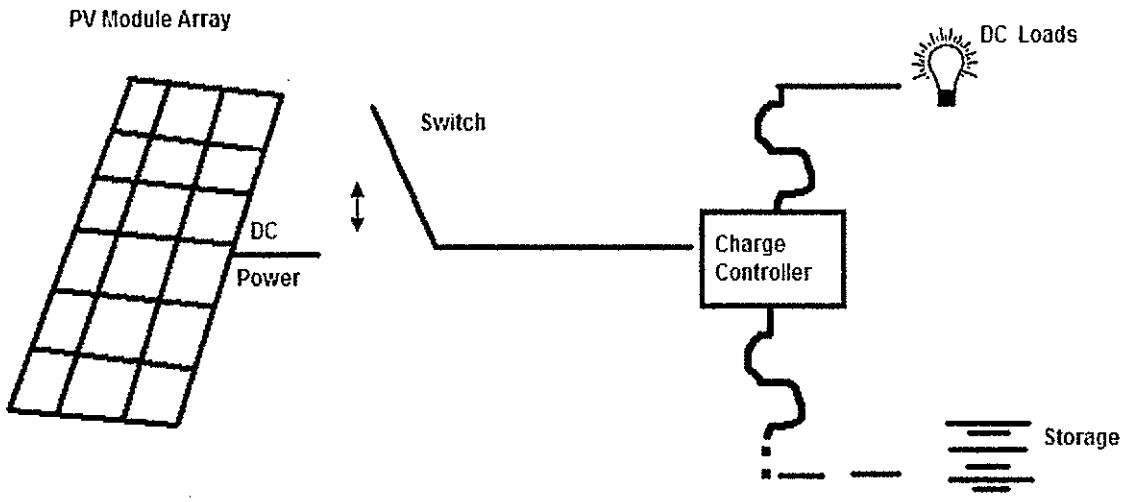

Figure 2.12: DC PV system Diagram [2].

AC off grid systems convert the DC energy to AC; and the loads runs directly on AC power. In addition, a voltage regulator is used to gauge the voltage to the connected loads. Remote homes that are not connected to electrical utility system utilize AC off grid systems. On grid PV systems converts the DC current to AC and this current is applied to a load or to a utility grid system. In order for a utility grid to take in AC current, the current AC voltage and frequency "must be synchronized" in phase with the interconnected utility system. Hybrid PV systems are systems that include PV systems and other connected "auxiliary sources of powers" [2] such as hydroelectric turbines and wind. Over all, well-built PV systems exhibit good performance, safety and reliability [2].

CHAPTER 3

SIMULATED TECHNIQUES

3.1 Introduction

With the growth of PV technology, there is a rising need to improve the PV system's output efficiency daily because of environmental conditions, i.e., day, night, cloud coverage, and shading from trees and building as the sun moving across the sky. One such method to improve efficiency employs maximum power point (MPPT) tracking. MPPT is "step size perturbation" that monitors the MPPT of PV systems via measuring the deltas of the output power over time and based on the deltas the output voltage is regulated [12]. Further enhancement to MPPT tracking involves the adaption of the Fibonacci Search Method. The research conducted in the following chapters of this work examines and investigates further MPPT approach using Fibonacci Search Method during conditions in which shading is present and not present at various times of the day as the sun moves across the sky. The research in this thesis uses existing mathematical models of PV systems and employs MPPT Fibonacci Search Method. In areas of the PV system where there is large shade coverage, the algorithm will alert the user to turn off that area of the array covered in shade while keeping the un-shaded areas on. This research examines the results of both techniques (turning off shading region and keeping the shaded regions on while observing the MPPT and output power. This chapter details two MPPT tracking techniques: Fibonacci Theory and Fibonacci Search Method.

3.1 Maximum Power Point tracking techniques

3.1.1 Perturbation and Observe (P&O) Method

P&O is an "iterative technique" to attain the MPPT by first assessing the PV system IV characteristics, next perturbing small voltage increments of the "operating voltage" (denoted as ΔVpv) of the PV system and monitoring the change in the output power, ΔPpv, looking for change in direction [12, 18]. A positive change in power denotes that the incremental voltage remains in the current direction the perturbation is going. However, if the change in power is negative, the incremental perturbation shifts to the reverse direction [18]. The algorithm tree diagram and the truth table of this method are shown in Figure 3.1 and Table 3.1, respectively.

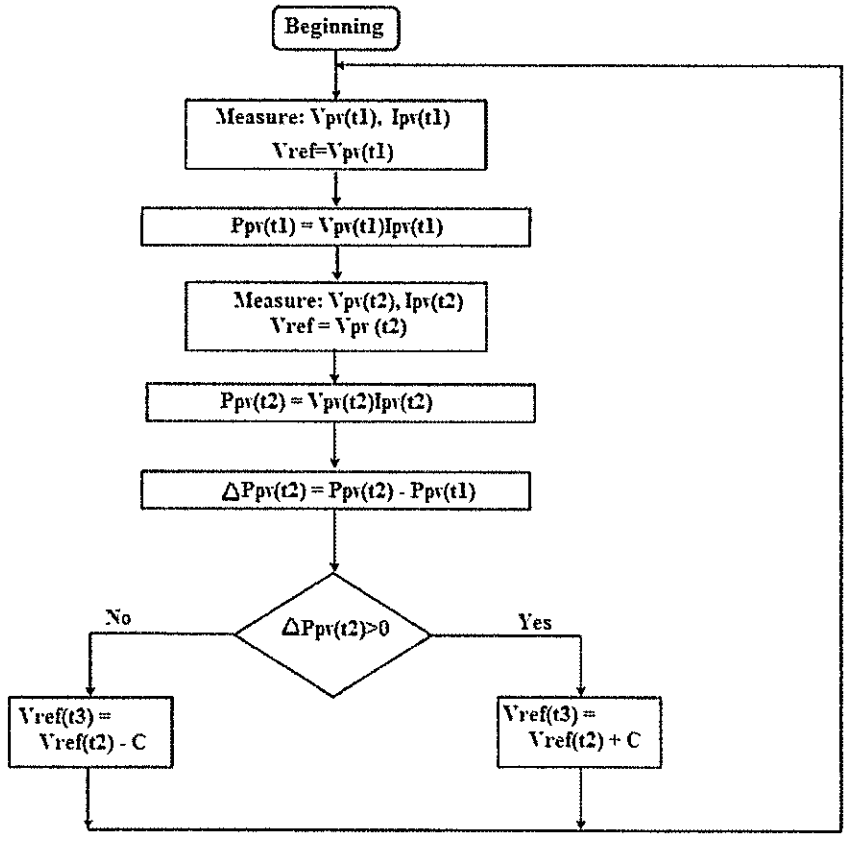

Figure 3.1: Flow Chart of Perturbation and Observed (P&O) Algorithm [18].

Table 3.1: P&O Truth Table [18].

Perturbation and Observe (P&O) Truth Table	
$\triangle \dot{P}_{pv}(t2)$	$V_{pv}(t3)$
> 0	"+"*
< 0	"_"*

* Note: "+" denotes an increase and "-" denotes a decrease

Another observation from Table 3.1 denotes that the perturbation voltage continuously increases if the change in power increases positively and the perturbation voltage will continue to decrease if the change in output power remains negative [18]. Drawbacks of using this method is the use of fixed increments perturbations. Fixed increments in the algorithm do not account for sudden increases or decreases in solar irradiance but still calculate the change with the previous step. This results in oscillatory and unreliable results of achieving the MPPT. Furthermore, using enhanced refine algorithm utilizing optimization techniques and variable perturbation in which the perturbation is dependent on the voltage duty cycle alleviates this issue [12].

3.1.2 Incremental Conductance (IC) Method

IC method utilizes the relationship between the MPPT voltage and the output voltage [12]. Consider the equation for the output voltage:

$$P = I * V \quad \text{(Eq. 3-1)}$$

$$\frac{dP}{dV} = I\frac{dV}{dV} + V * \frac{dI}{dV}, \quad \text{(Eq. 3-2)}$$

$$\frac{dP}{dV} = I + V * \frac{dI}{dV}. \quad \text{(Eq. 3-3)}$$

Recall back in Chapter 2 that MPPT is achieved when $\frac{dP}{dV} = 0$.

$$\frac{dP}{dV} = I + V * \frac{dI}{dV} = 0, \quad \text{(Eq. 3-4)}$$

$$I + V * \frac{dI}{dV} = 0 \rightarrow I = -V * \frac{dI}{dV}, \quad \text{(Eq. 3-5)}$$

$$-\frac{I}{V} = \frac{dI}{dV}. \quad \text{(Eq. 3-6)}$$

Equation 3-6 denotes that the "opposite value of the conductance" is equal to the change of the incremental conductance [12].

Furthermore, dI and dV are calculated via ΔPpv and ΔVpv as P and V are measured (as described in Section 3.1.1) from previous perturbation increment.

$$dV\ (t2) \approx \Delta Vpv\ (t2), \quad \text{(Eq. 3-7)}$$

$$\Delta Vpv\ (t2) = Vpv(t2) - Vpv(t1), \quad \text{(Eq. 3-8)}$$

$$dI(t2) \approx \Delta Ipv\ (t2), \quad \text{(Eq. 3-9)}$$

$$\Delta Ipv\ (t2) = Ipv(t2) - Ipv(t1). \quad \text{(Eq. 3-10)}$$

The tree algorithm for IC method is shown in Figure 3-2.

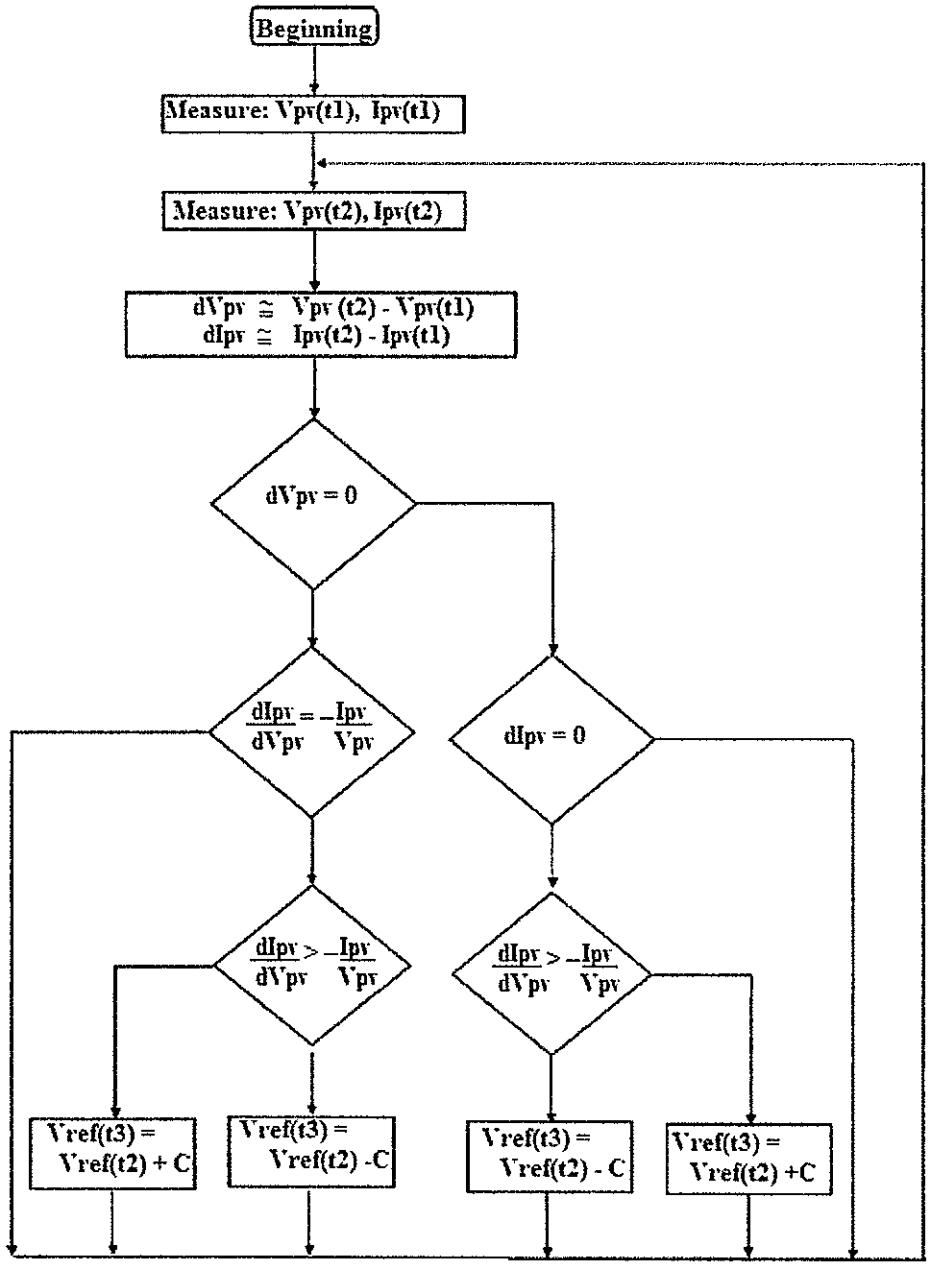

Figure 3.2: Flow Chart of IC Algorithm [12].

Results of this algorithm reveal:

- If $\frac{dP}{dV} < 0$ $(\frac{dI}{dV} < -\frac{I}{V})$, then the operating voltage is greater than the MPPT voltage [12],

- If $\frac{dP}{dV} = 0$ ($\frac{dI}{dV} = -\frac{I}{V}$), then the operating voltage equates to the MPPT voltage [12],
- If $\frac{dP}{dV} > 0$ ($\frac{dI}{dV} > -\frac{I}{V}$), then the operating voltage is smaller than the MPPT voltage [12].

Based on these results, the operating voltage is regulated according to the value of the MPPT voltage. This method, while more complex, has advantages over the P&O method in that it adapts faster to dramatic environmental changes such as solar irradiance, temperature, and cloud coverage and thus results in smaller "oscillation around MPPT than P&O" [12, 18]. Setting ΔVpv initially at a high value reduces the "tracking accuracy"; on the other hand, setting ΔVpv too low slows down the "tracking speed" and thus lowers the PV efficiency [18].

3.2. Optimization

3.2.1 Optimization Background

Optimization is a mathematical procedure from first year calculus in which a function under set conditions is maximized or minimized. Earliest recorded optimization technique using calculus in the European world traces back to 1847 with Cauchy. Cauchy introduced minimization optimization via the use of derivatives (or gradients). Later different mathematician published different papers on expounding upon various optimization methods. In 1951, Dantzig published a paper "on the simplex method" using linear programming. Between 1939 and 1951, Karush, Kuhn, and Tucker developed a method concerning "optimality conditions for constrained problems" [1]. Later in the 1960s, mathematicians derived numerical methods to resolve nonlinear optimization

problems. During the 1970s, Fibonacci numbers followed by the Golden Section Ratio were used as optimization method concerning "interval search methods" [1].

3.2.2 Fibonacci Background

The first and earliest documentation of Fibonacci numbers is traced back to India in 200 BC from works of Pingala and later to 700 AD from the works of Virahanka. Leonardo of Pisa, also known as Fibonacci, revealed Fibonacci numbers to "Western European Mathematics" in 1202 via his book *Liber Abaci*. Fibonacci derived these numbers in studying rabbits' reproduction by observing the period of rabbits' reproduction and their offspring [1].

3.2.2.1 Fibonacci Theory

Fibonacci numbers also called Fibonacci series and sequence are all terms used to describe the sequence of integer "0, 1, 1, 2, 3, 5, 8..." or "1, 1, 2, 3, 5, 8, 12..." The first number of the non-negative integer sequence begins with a zero or one and the rest of the numbers in the sequence follows the Equation 3-11 [15]:

$$F_0 = 0,\ F_1 = 1 \qquad F_n = F_{n-1} + F_{nn-2} \qquad \text{for all } n \geq 2 \qquad \text{(Eq. 3-11)}$$

3.3 Optimization Search Algorithm Technique: Fibonacci Search Algorithm

3.3.1 Fibonacci Method

This mathematical method is used when there is a need to shorten "the interval of uncertainty" or "the interval containing the minimum" to a certain value in the smallest number of runs or "function evaluations." Suppose there is uncertainty within the

interval 5-8. Two points such as six and seven are revealed to be within this interval. Knowing the certainty of these two points, three cases surface:

Case 1: If f6 < f7, then 5-7 is the new interval of uncertainty,

Case 2: If f6 > f7, then 6-8 is the new interval of uncertainty, points 6 and 7 becomes 5 and 6 respectively; and f2 now becomes f3, as shown in Figure 3.3 [1]

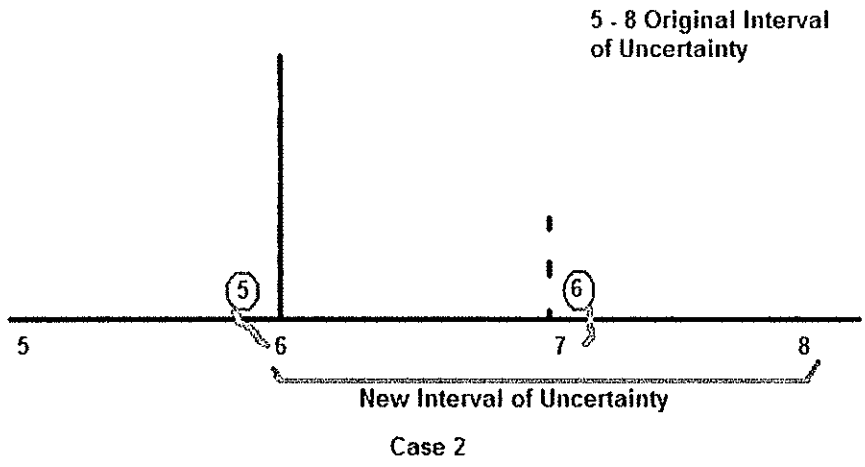

Figure 3.3: Interval Reduction Case 2 [1].

Case 3: If f6 = f7 either case 1 or case 2 is applied with equal probable chance of occurring.

After the appropriate case is selected, a new point is reveals and further reduction takes place with the interval. However, the new point is introduced such that the length of interval 5-7 and 6-8 is the same [1].

3.3.2 Fibonacci Search Method Example

This section provides an example using Fibonacci Search Algorithm to determine the maximum of the function of the given function within the function $0 \leq x \leq 2$:

$f(x)=-(x-1)^2+1$ within the interval $0 \leq x \leq 2$. (Eq. 3-12)

The graph of the function is shown in Figure 3.4,

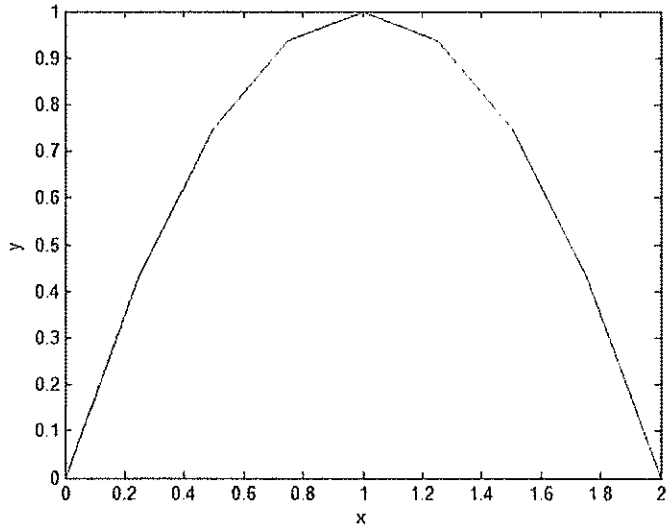

Figure 3.4: Graph of $f(x)=-(x-1)^2+1$.

Next, we populate our four place holder numbers x1, x2, x3, and x4. Two check points x2 and x3 are determined at random within the interval; it is important to note that x1 will always be less than x2 when choosing the values. Therefore x1 is 0.2 and x2 is 1.75. x3 and x4 are two extremity points of the function; x3 is always smaller than x1 and x4 is always greater than x2. Our x3 value is 0 and our x4 value is 2. Now we have four numbers used in the Fibonacci Search shown below, Figure 3.5, $x3=0 < x1=0.2 < x2=1.75 < x4=2$.

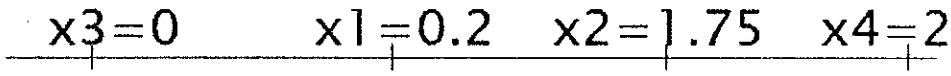

Figure 3.5: Line Graph of the Four Values used in the Fibonacci Search.

Next F(x1=0.2) and F(x2=1.75) is calculated to be 0.36 and 0.4 respectively. These two values are compared and is the first iteration of the search. Since F(x2)>F(x1), the range shifts to the right and our three place holder values are updated, where x1 becomes x3 (x3=(x1=0.2)), x2 becomes x1 (x1=(x2=1.75)), and x2 is computed using the following Equation 3-13 (similar to Equation 3-12 above):

$$x2 = x3 + \frac{F(n-1)}{F(n)}(x4 - x3)\text{ , where n=2,} \qquad \text{(Eq. 3-13)}$$

$$x2 = 0.2 + \frac{1}{1}(2 - 0.2) = 2. \qquad \text{(Eq. 3-14)}$$

The value of x4 remains the same since x4 there is not value to the right for x4 to shift to a visual representation of the shift is given in Figure 3.6.

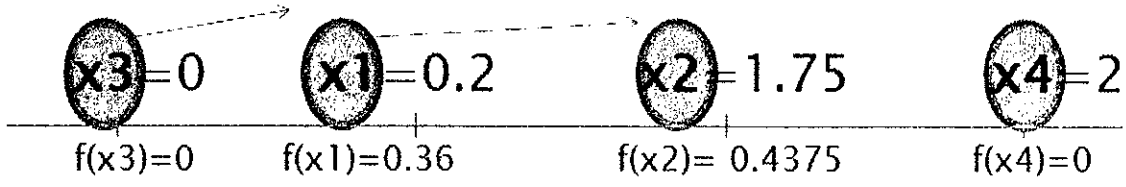

Figure 3.6: Visual Representation of Shift to Right Run 1.

The updated line graph of the four place holder values is given in Figure 3.7.

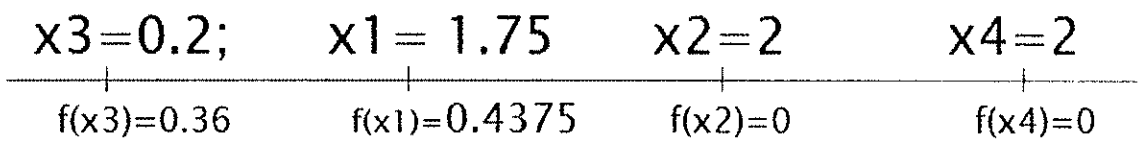

Figure 3.7: Line Graph of the Four Values used in the Fibonacci Search Run 1.

Next, we are at run 2 of the search algorithm, and x1 and x2 are evaluated in the same function, where F(x1)=0.36 and F(x2)=0. Comparing F(x1) and F(x2), it is determined that F(x1)> F(x2), and so the interval is shifted to the left. The value in x4 now takes on the value of x2 (x4=(x2=2)), x2 now takes the value of x1 (x2=(x1=1.75)). The value of x1 is computed using the equation given in (3-15)

$$x1 = x4 - \frac{F(n-1)}{F(n)}(x4 - x3), \text{ where n=3,} \qquad \text{(Eq. 3-15)}$$

$$x1 = 2 - \frac{1}{2}(2 - 0.2) = 1.1. \qquad \text{(Eq. 3-16)}$$

The value of x3 remains the same because x3 is the last place holder used in this algorithm and thus cannot be shifted to the left. Visual representations of this left shift followed by the line graph are shown in Figures 3.8 and 3.9, respectively.

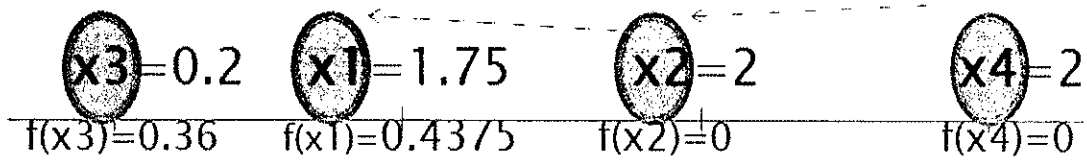

Figure 3.8: Visual Representation of Shift to left Run 2.

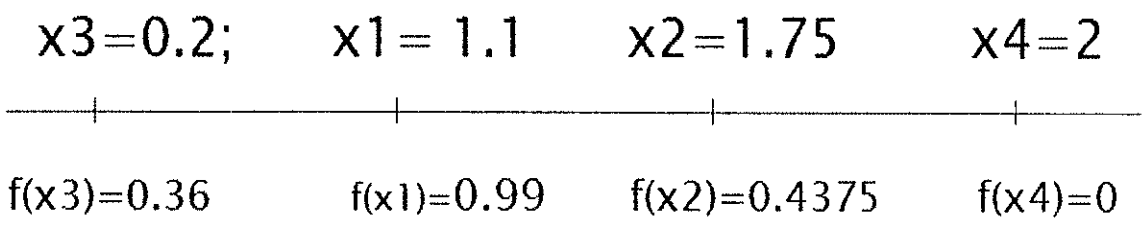

Figure 3.9: Line Graph of the Four Values used in the Fibonacci Search Run 2.

We are now at run 3, where we again evaluate F(x1) = 0.99 and F(x2) =0.4375 and compare. Since F(x1)> F(x2), the interval shifts to the left again, where x4 takes on the value x2 (x4=(x2=1.75)), x2 takes the value of x1 (x2 = (x1=1.1)), and x1 is computed using the Equation 3-15 .

$$x1 = 1.1 - \frac{2}{3}(1.75 - 0.3) = 0.7167 \text{ where n=4 .} \qquad \text{(Eq. 3-19)}$$

The value of x3 remains the same because x3 is the last place holder used in this algorithm and thus cannot be shifted to the left. Visual representations of this left shift followed by the line graph are shown in Figures 3.10 and 3.11, respectively.

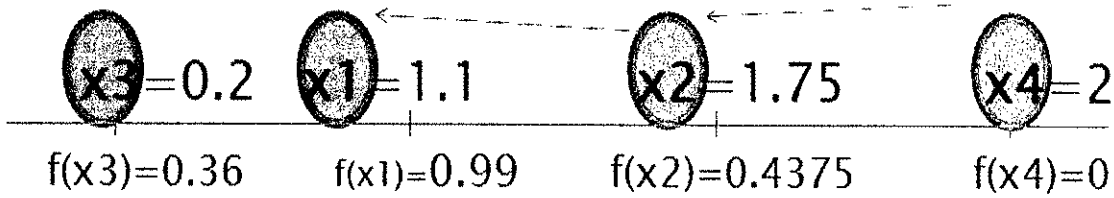

Figure 3.10: Visual Representation of Shift to left Run 3.

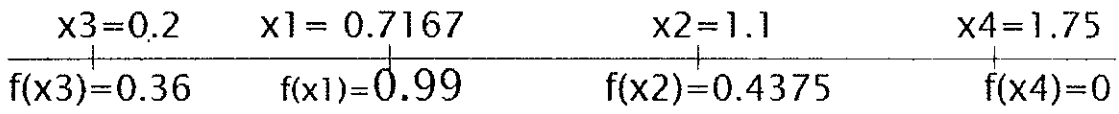

Figure 3.11: Line Graph of the Four Values used in the Fibonacci Search Run 3.

These iterations repeats with applicable runs to the left and to right until there is little to no change in the computed function of F(x1) and F(x2), thus the maximum is known. Table 3.12 gives us the complete results of the calculated, where Power(x1) and Power(x2) represents F(x1) and F(x2), respectively.

	A	B	C	D	E	F	G
1	Run	Power(x1)	Power(x2)	x3	x1	x2	x4
2	1	0.36	0.4375	0	0.2	1.75	2
3		Shift to right		0.2	1.75	2	2
4	2	0.4375	0	0.2	1.75	2	2
5		Shift to left		0.2	1.1	1.75	2
6	3	0.99	0.4375	0.2	1.1	1.75	2
7		Shift to left		0.2	0.7167	1.1	1.75
8	4	0.9197	0.99	0.2	0.7167	1.1	1.75
9		Shift to right		0.7167	1.1	1.3367	1.75
10	5	0.99	0.8867	0.7167	1.1	1.3367	1.75
11		Shift to left		0.7167	0.9492	1.1	1.3367
12	6	0.9974	0.99	0.7167	0.9492	1.1	1.3367
13		Shift to left		0.7167	0.8641	0.9492	1.1
14	7	0.9815	0.9974	0.7167	0.8641	0.9492	1.1
15	8	0.9974	0.9999	0.8641	0.9492	1.0101	1.1
16	9	0.9999	0.9982	0.9492	1.0101	1.0423	1.1
17	10	0.9998	0.9999	0.9847	1.0101	1.0203	1.0423
18	11	0.9999	0.9996	0.9847	0.9983	1.0101	1.0203
19	12	1	0.9999	0.9847	0.9944	0.9983	1.0101
20	13	1	1	0.9944	0.9983	1.0041	1.0101
21	14	1	1	0.9944	0.9981	0.9983	1.0041
22	15	1	1	0.9981	0.9983	1.0018	1.0041
23	16	1	1	0.9981	0.9996	0.9983	1.0018

Figure 3.12 Results of the Fibonacci Method to Determine the Function maximum.

The circled values represent the position of the left or right shifts. We know that the maximum of the function is at (x=1, y=1), and reviewing Figure 3-8, we see that the maximum value was determined at run 13, where both F(x1) and F(x2) are equal.

3.3.3 Fibonacci Search Algorithm

This algorithm is a "divide and conquer" method that base its search pattern on Fibonacci numbers. This method minimizes excessive probable positions via incessantly contracting the interval. As the interval narrows, an optimal point will always stay in that interval and thus shifting, "to the left or to the right" will take place within the interval. The direction of this interval shift depends "on the values of that function at two check points, p1 and p2" [15].

Let there be four points, p1, p2, p3, and p4, p3 < p1 < p2 < p4, a pictorial layout of these four points is shown in Figure 3.13. Moreover, p1 and p2 are the check points in this range, while P3 and P4 are outlier points or "extremities" on the end of the interval range. The following equation represents the range of the four points [15]:

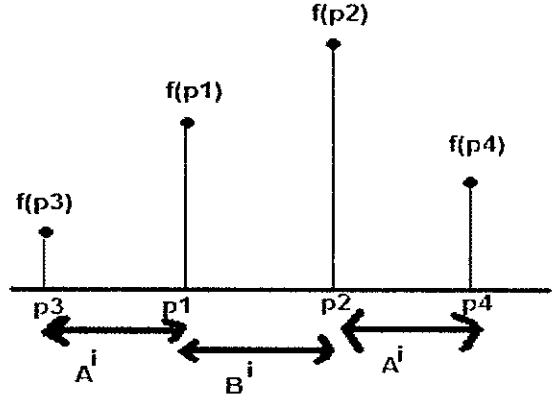

Figure 3.13: Initial Range Layout before use of Fibonacci Search Method [15]

$$A^i + B^i + A^i = T^i. \quad \text{(Eq. 3-20)}$$

Points p1 and p2 are first examined in the search, and because p2 >p1; the interval moves to the right with p3=p1, and p1=p2. Figure 3.14 shows the updated pictorial diagram after the Fibonacci Search. The following equation is used to calculate the updated and replacement value of p2 [15]:

$$p2 = p3 + \left[\frac{F(n-1)}{F(n)}\right][p4 - p3]. \quad \text{(Eq. 3-21)}$$

The new equation for the range:

$$A^{i+1} + B^{i+1} + A^{i+1} = A^i + B^i = T^i - A^i. \quad \text{(Eq. 3-22)}$$

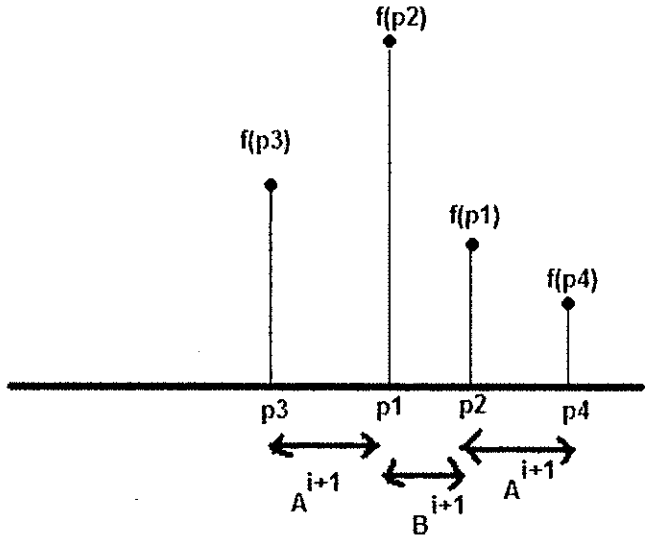

Figure 3.14: Updated Range Layout after first iteration of Fibonacci Search Method [15].

Now, p3 < p2 < p1 < p4; examining the two checkpoints p1 and p2, since p2 < p1, the interval now moves to the left and p2 = p1, and p4 = p2 [15]. The following equation updates the value for p1 [15]:

$$p1 = p4 + \left[\frac{F(n-1)}{F(n)}\right][p4 - p3], \quad \text{(Eq. 3-23)}$$

3.3.4 MPPT Fibonacci Search Algorithm

The Fibonacci Search Method in PV systems follows the same approach where pi is now the voltage and F(pi) is the power. As before, the first step sets the two voltages which are the "optimal points". As described in the previous section, these voltage values are evaluated and are appropriately moved to right or left or right. Next, the respective updated voltage value is determined, and the search algorithm repeats with the next iteration of the search. This procedure repeats until the MPPT value found. A refine layout of this search follows these steps and the diagram is shown in Figure 3.15 [15]:

1) Set the variables,

2) "Measure the power"

3) Assess and compare the power with the preceding value or set MPPT value. Move to step 4 if the difference in power is larger than the "power ripple"; otherwise if this difference is not larger than the "power ripple" repeat step 3.

4) Declare and Set the two voltages V1, and V2.

5) Calculate and determine via measurements the respective powers P1, and P2.

6) If P1 larger than P2, "shift to the left, else move to the right."

7) Calculate and determine the appropriate updated values for V1 or V2.

8) Determine via measurements the respective power value of the updated voltage V1 or V2.

9) Start back at step 6 [15].

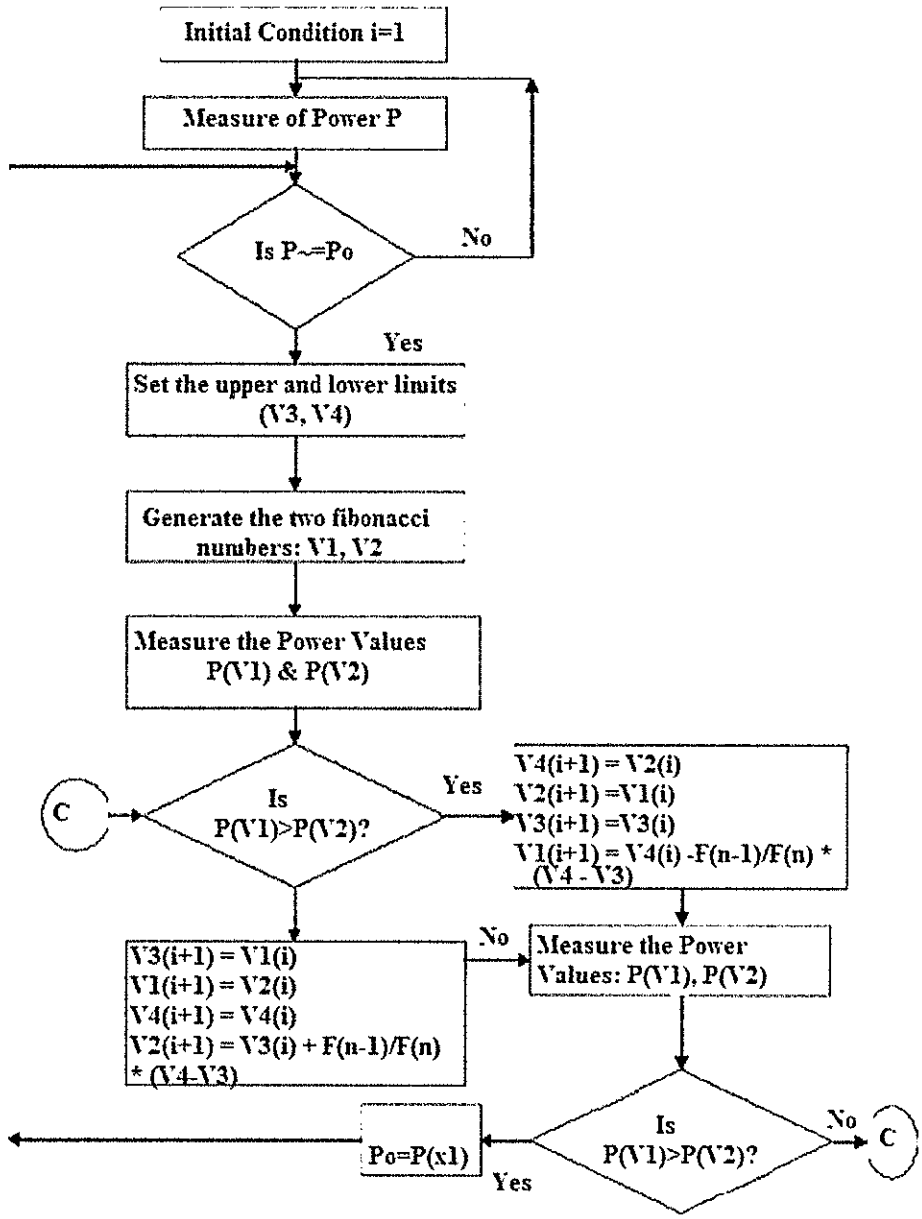

Figure 3.15: Flow Chart of Fibonacci Search Algorithm for PV Systems [15]

3.3.5 MPPT Fibonacci Search Algorithm 1x5 Array Example

This section gives a step by step example of a sampled 1x5 PV array using two methods, Fibonacci Full Search Algorithm, also denoted as Full Search and Fibonacci Quick Search Algorithm also denoted as Quick Search in this thesis. These two methods

were used in calculating the MPPT in this research and the results of the two methods are discussed in Chapter 4. Figure 3.16 and Figure 3.17 depict two representations of same 5x5 array. Figure 3.16 reveals the voltage values in volts of each of the five cells in the 5x5 array, and Figure 3.17 reveals the current values in amperes. The two figures are the first rows of the 5x5 PV arrays given in Chapter 4, Figure 4.1 and 4.2, where again Figure 4.1 depicts the voltage values of each individual cells in volts of the 5x5 Array, and Figure 4.2 is the current values of each cell in amperes.

Voltage				
11	12	13	14	12

Figure 3.16: Voltage Values in Volts of each Cell in the 1x5 Array.

Current				
1.712	1.711	1.711	1.711	1.711

Figure 3.17: Current Values in Amperes of each Cell in the 1x5 Array.

Going through the algorithm shown in Figure 3.15, let us assume that we have already set the initial conditions, measured the power, and compared this power with the output power.

3.3.6 MPPT Fibonacci Full Search Algorithm 1x5 Array Example

For the Full Search, we set the upper and lower limits, (in the previous example from Section 3.5 this is the extremity points). The value of the upper and lower limits are the first two elements in the array $V3^1$ is 11 volts (the first row and first column of the 1x5 Array) and $V4^1$ is 12 volts (the first row, second column of the 1x5 Array). We now generate $V1^1$ and $V2^1$ using the same calculations from Equations 3-21 and 3-23. The superscripts of V1-V4 depict the index number of the V1-V4 and it tells us where the values are stored, noticed that V1, V2, V3 and V4 are analogous to X1, X2, X3, and X4 above. $V1^1$ and $V2^1$ are computed using Fibonacci Numbers

$$V1^1 = V4^1 - \frac{F(n-1)}{F(n)}(V4^1 - V3^1), \text{ where n=3,} \quad \text{(Eq. 3-24)}$$

$$V1^1 = 12 - \frac{1}{2}(12 - 11) = 11.5\ volts, \quad \text{(Eq. 3-25)}$$

$$V2^1 = V3^1 + \frac{F(n-1)}{F(n)}(V4^1 - V3^1), \text{ where n=3,} \quad \text{(Eq. 3-26)}$$

$$V2^1 = 11 + \frac{1}{2}(12 - 11) = 11.5\ volts. \quad \text{(Eq. 3-27)}$$

It is important to note, the rule holds true $V3^1 < V1^1 < V2^1 < V4^1$ of the computed interval. Run one starts, with measuring the power denoted as $P1^1$ and $P2^1$. The current values used to calculate the power are the current values in the first and second elements of the 1x5 array given in Figure 3.17; they are denoted as $I1^1$ and $I2^1$.

Therefore, as $P1^1$ and $P2^1$ are shown below.

$$P1^1 = V1^1 \times I1^1 = 11.50 \times 1.712 = 19.69\ Watts, \quad \text{(Eq. 3-28)}$$

$$P2^1 = V2^1 \times I2^1 = 11.50 \times 1.711 = 19.68\ Watts. \quad \text{(Eq. 3-29)}$$

$P1^1$ and $P2^1$ values are then compared and depending on the comparison the interval shifts to the left or to the right. In this first run, $P1^1$ is greater than $P2^1$ and so the interval

shifts to the left. Just as in the previous example, $V4^2$ takes the value of $V2^1$ ($V4^2$=$V2^1$=11.5 V), $V2^2$ takes the value of $V1^1$ ($V2^2$=$V1^1$=11.5 V), $V3^2$ remains the same as $V3^1$ ($V3^2$= $V3^1$=11.00V. $V1^2$is computed using the equation 20, but now n=4. (note 2 in the subscript is not exponent, but denotes the index number)

$$V1^2 = V4^2 - \frac{F(n-1)}{F(n)}(V4^2 - V3^2), \text{ where n=4,} \quad \text{(Eq. 3-30)}$$

$$V1^1 = 11.5 - \frac{2}{3}(11.5 - 11) = 11.17\ volts\ . \quad \text{(Eq. 3-31)}$$

Note that the rules still holds valid, where $V3^2 < V1^2 < V2^2 = V4^2$. Next, run 2, $P1^2$ and $P2^2$ are computed.

$$P1^2 = V1^2 \times I1^2 = 11.17 \times 1.712 = 19.12\ Watts, \quad \text{(Eq. 3-32)}$$

$$P2^2 = V2^2 \times I2^2 = 11.50 \times 1.711 = 19.68\ Watts. \quad \text{(Eq. 3-33)}$$

$P1^2$ and $P2^2$ are compared, and since $P2^2$ is greater than $P1^2$, the interval shifts to the right. Therefore, $V3^3$ takes the value of $V1^2$ ($V3^3$=$V1^2$=11.17 V), $V1^3$ takes the value of $V2^2$ ($V1^3$=$V2^2$=11.5 V), $V4^3$ remains the same as $V4^2$ ($V4^3$= $V4^2$=11.50V. $V2^3$is computed using the Equation 3-34, but now n=5.

$$V2^3 = V3^3 - \frac{F(n-1)}{F(n)}(V4^3 - V3^3), \text{ where n=5,} \quad \text{(Eq. 3-34)}$$

$$V2^3 = 11.17 - \frac{3}{5}(11.5 - 11.17) = 11.37\ volts. \quad \text{(Eq. 3-35)}$$

Next, run 3, $P1^3$ and $P2^3$ are computed.

$$P1^3 = V1^3 \times I1^3 = 11.50 \times 1.712 = 19.69\ Watts, \quad \text{(Eq. 3-36)}$$

$$P2^3 = V2^3 \times I2^3 = 11.37 \times 1.711 = 19.44\ Watts. \quad \text{(Eq. 3-37)}$$

The computations of $P1^1$ and $P2^2$ are invalid, since $V3^3 < V1^3 \not< V2^3 < V4^3$. Therefore, as shown in Figure 3.18, the algorithm goes out the loop.

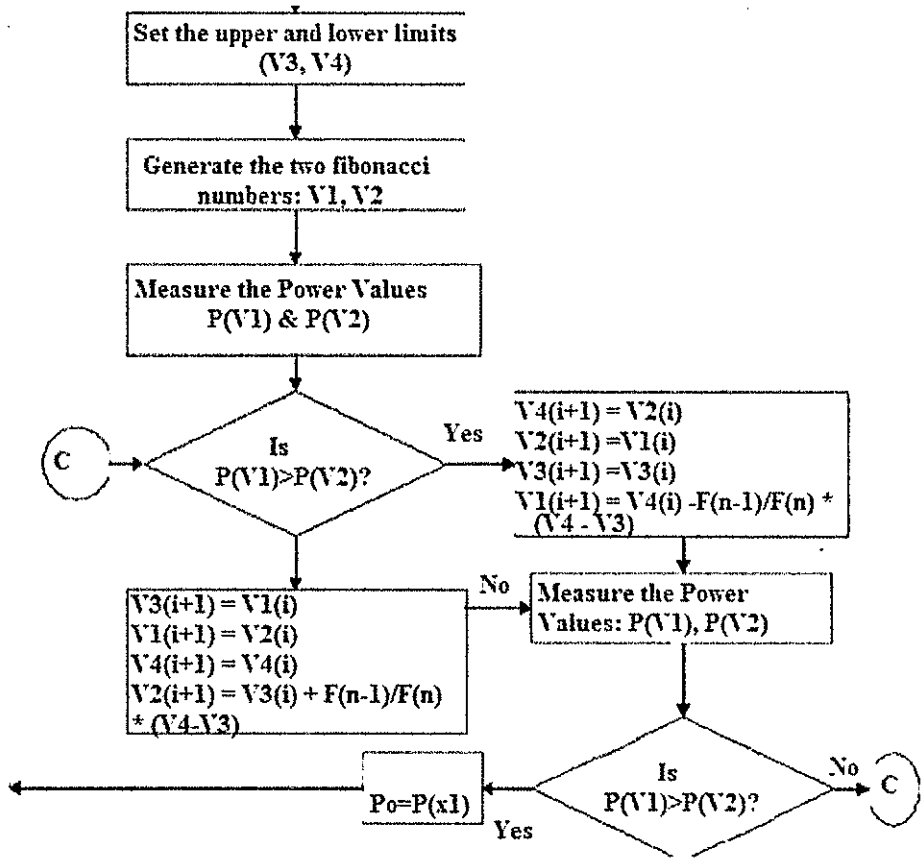

Figure 3.18: Cropped Flow Chart of Fibonacci Search Algorithm for PV Systems [15].

Next, we take the next two values from voltage array in Figure 3.16 and store them as $V3^3$ and $V4^3$. Therefore, $V3^3 = 12$ volts and $V4^3 = 13$ volts and the steps in the algorithm shown in Figure 3.5, repeats until the interval rule $V3^3 < V1^3 < V2^3 < V4^3$ becomes invalid and the values for V3 and V4 values are pulled from the array. This process continues until the last, (ith, jth), element in the array is stored in $V3^n$; to account for the nth position of $V4^n$ the (i-1, j-1) value is taken. In other words, the (ith,jth) position of the 1x5 array is (1,5) which is the value of 12. This value is stored in $V3^n$; $V4^n$ takes the (i, j-1) value of the array which for our 1x5 example is (1,4) position and is 14 volts.

3.3.7 MPPT Fibonacci Quick Search Algorithm

The Fibonacci Quick Search Algorithm follows the same algorithm as the flow chart in Figure 3.15; however, the only difference here is how the algorithm pulls the values from the array. The Quick Search Algorithm used Fibonacci Numbers for the jth position of the voltage and current values. Reviewing the Fibonacci sequence:

0,1,1,2,3,5, 8…..F(n)+F(n-1) with n=1,2,3,4…n. (Eq. 3-38)

We start with n=3rd position of the sequence because there cannot be 0 position (n=1), and there cannot be duplicate position of 1 and 1 (n=2 and n=3, respectively) for j. Therefore, reviewing the voltage and current values of the PV 1x5 array given in Figures 3.16 and 3.17 respectively, where in (i,j)the ith position is the row number and the jth is the column number. The j position is the 3rd position of the Fibonacci sequence which is 1, so j=1 for $V3^1$ which is the (1,1) position of the array, 11 volts. The value stored in $V4^1$ variable is the j+1th position which is (1,2) position of the array, 12 volts. Using the same algorithm and computation as in Section 3.3.6, the algorithm continues until the interval $V3^2 < V1^2 < V2^2 < V4^2$ becomes invalid. When invalid, the next two values are taken from the array, where index j is the 4th (n=4) position of the Fibonacci sequence which is two. So, V3=12 volts, and V4 takes the j+1 position of the array which is 13 volts. When n=5 in the Fibonacci sequence, j is now 3, so position (1,3) makes V3= 13 Volts and j+1 is 4, so position (1,4) makes V4=14 volts. At n=6 in the Fibonacci sequence, j is now 5, so position (1,5) makes V3= 12 volts. Because there is no j+1, we are at the last element of the row, we now use j-1 position, (1,4), for V4 so position (1,4) makes V4=14 volts. If this array was bigger, or 1x10 array, for example, the next value in the array will pull from n=7 of the Fibonacci number which is 8; therefore j will equal

8 in the (i^{th},j^{th}) position of the array for V3 and j+1 will equal 9 in the [i^{th}, $(j+1)^{th}$] position of the array for V4. It is important to note that unlike the Full Search, the Quick Search does not examine every element in the array, but uses Fibonacci Numbers as its jth value in the column of the array. For larger arrays where the number of rows is greater than or equal to two, the array is concatenated into a px1 string, and we use p^{th} and $(p+1)^{th}$ positions of this string according to the ni^{th} position of the Fibonacci Sequence.

CHAPTER 4

SIMULATION RESULTS AND DISCUSSION

4.1 Introduction

In this chapter, details of the simulation results obtained from Matlab are discussed. The methods described in the previous chapter were used for the numerical calculations. The main goal of this work is to observe the maximum power point and the number of iterations taken to compute the maximum power point value using the Full and Quick Fibonacci Search Algorithms. In addition, once the MPPT value was calculated, this MPPT value was compared to the other values of the solar cells, and the individual cells that had output values at half the MPPT, were turned off. Three PV systems of different sizes were represented and the voltage and current values of each solar cell was aggrandized into a matrix text file. It is important to note the assumption that the numerical voltages and currents values represent the voltage and current of each solar cell at a given time during the daylight hours. As discussed in the previous chapter, the Matlab file reads the represented PV voltages and current from the text files. These values were used in the Full and Quick Fibonacci Search Algorithm's Matlab functions to determine the MPPT. The results of the Full and Quick searches are compared and discussed.

4.2 5x5 Solar Array Results

The first array modeled was a five by five solar cell array. Tables 4.1 and 4.2 depict the numerical voltages and current values of the 5x5 PV array, where each entry in the matrix represents a PV cell.

Table 4.1: Trial 1- Voltage Values of 5x5 PV Array.

Voltage (in Volts) Values of 5x5 Solar Array				
11	12	13	14	12
10	12	14	11	13
36	33	32	31	30
34	30	31	32	36
36	38	39	37	30

Table 4.2: Trial 1- Current Values of 5x5 PV Array.

Current (in Ampere) Values of 5x5 PV Array				
1.712	1.711	1.711	1.711	1.711
1.711	1.712	1.712	1.711	1.711
1.712	1.711	1.711	1.711	1.712
1.712	1.711	1.711	1.711	1.711
1.712	1.712	1.711	1.711	1.711

To provide a visual representation, bar plots of the voltage and power values for each cell in the array are shown in Figures 4.1 and 4.2, respectively. Both images in Figure 4.1 are the same, but rotated to give different views of the array, and the same goes for the bar plots shown in Figure 4.2. In the bar plot, the x and y axes represent the rows and columns of the array, respectively, and the z axis denotes the voltage in volts.

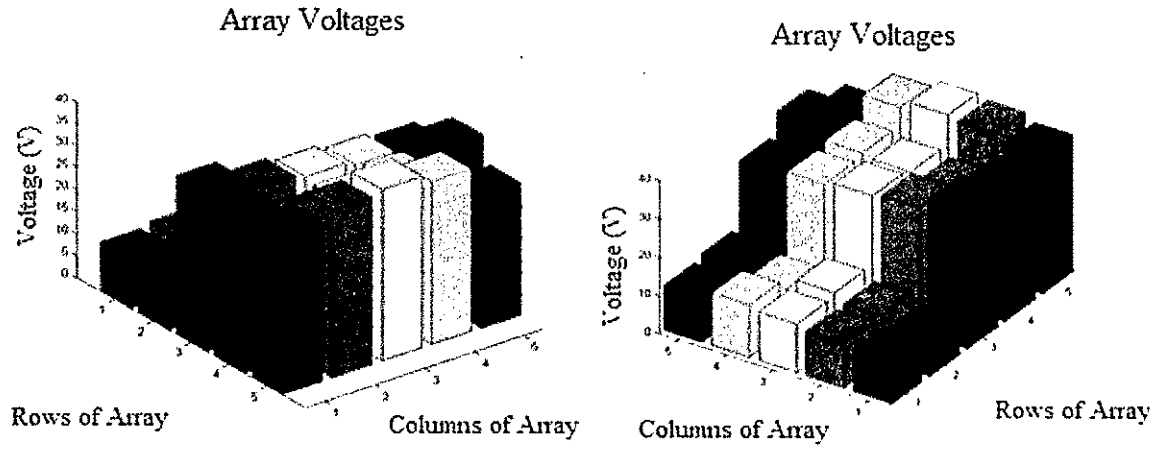

Figure 4.1: Trial 1 Bar Plots of the Voltages of each Cell in the 5x5 PV Array.

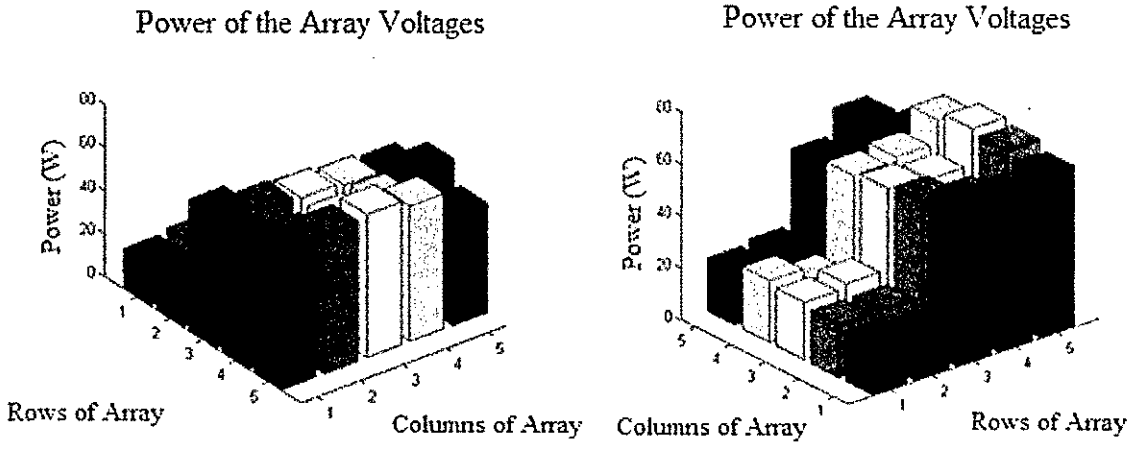

Figure 4.2: Trial 1 Bar Plots of the Power of each Cell in the 5x5 PV Array.

Therefore, entry row one, column one also denoted as (1, 1) in Table 4.1 with a value of 11 (Volts) is also seen in the second right bar plot in Figure 4.1 by locating the x and y position of the 1st row and the 1st column. Same description applies to the power values in Figure 4.2, with the x and y position related to the product of the PV cells in Tables 4.1 4.2.

4.2.1 Full Search Results

The Fibonacci Full Search Algorithm output the voltage values and the respective power values. These values were written to an Excel file, shown in Table 6. Column A represents the voltage values in volts, Column B represents the power values in watts, and the left side (cell's row number of the field) shows the nth iteration number, where the true iteration number is the Excel's row number minus one.

Table 4.3: Trial 1a MPPT Full Search Voltage and Power Data Results.

	A	B
1	Voltage(V)	Power(Watts)
2	11.5	19.688
3	11.1667	19.1173
4	12.5	21.3875
5	12.1667	20.8172
6	13.5	23.0985
7	13.5	23.0985
8	12	20.532
9	12	20.532
10	12	20.532
11	11	18.821
12	10.3333	17.6803
13	13	22.243
14	13	22.243
15	11	18.821
16	11	18.821
17	11	18.821
18	11	18.821
19	33	56.463
20	32	54.752
21	31	53.041
22	30	51.33
23	30	51.33
24	30	51.33
25	30	51.33
26	31.5	53.8965
27	31.5	53.8965

	A	B
27	31.5	53.8965
28	34	58.174
29	34	58.174
30	32	54.752
31	36	61.596
32	38.5	65.8735
33	38.5	65.8735
34	37	63.307
35	37	63.307
36	37	63.307
37	37	63.307
38	37	63.307
39	30	51.33
40	30	51.33
41	37	63.307

As shown in the results of Table 4.3, Fibonacci Full Search Algorithm went through the entire 5x5 Array, and the Maximum Power Point (MPP) Value was found between the 31st and 32nd run. In other words, it took 31st and 32nd iterations to compute

and track the Full Search Algorithm's Maximum Power Point Value of 65.8735 watts in the 5x5 array. The actual maximum power calculated from taking the maximum voltage and current values of 39 volts and 1.711 amperes from Table 4.1 and 4.2 is 66.729 watts. The power values and respective run numbers are plotted and shown in Figure 4.3. Figure 4.4 depicts power versus voltage graph.

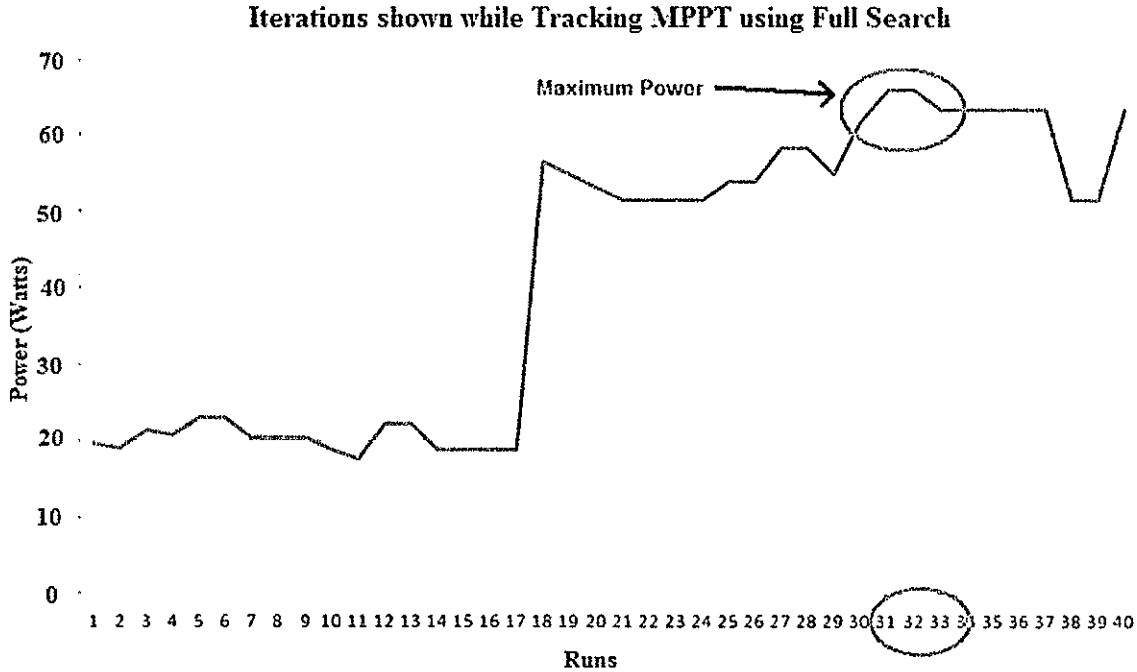

Figure 4.3: Trial 1a MPPT Iterations using Full Search.

Analogous to the Excel data values, the maximum power value is shown to be 65 watts computed on the 31st and 32 run. Figure 4.4 reveals the MPPT with its respective voltage value at 38.5 volts.

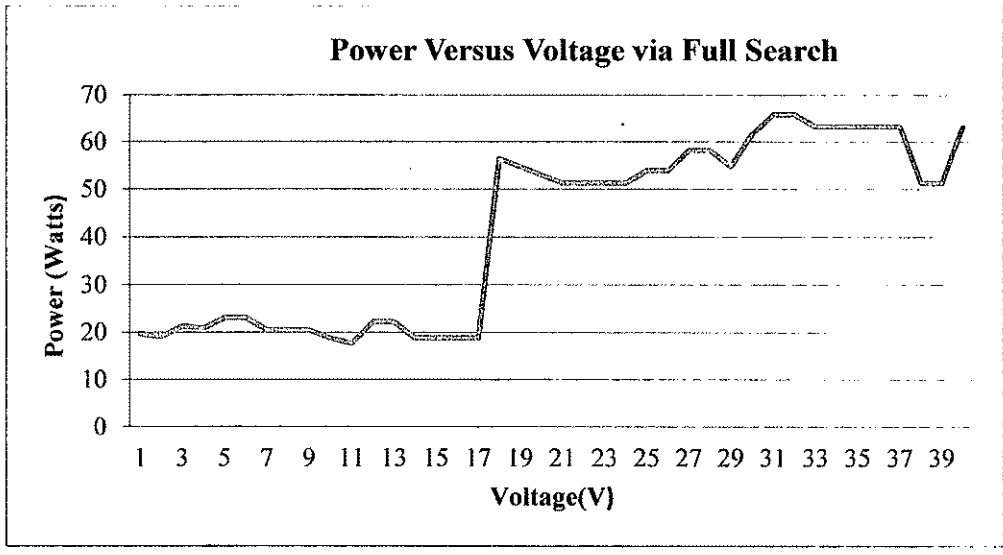

Figure 4.4: Trial 1a Power versus Voltage using Full Search.

The algorithm calculated the Maximum Power 65.87 watts, searched every array, and also turned off the cells that were outputting half of the MPP value. The resulting 5x5 PV array is depicted in Figure 4.5. As seen from a comparison with Figure 4.2, the first two rows output the lowest power, and thus these were turned off.

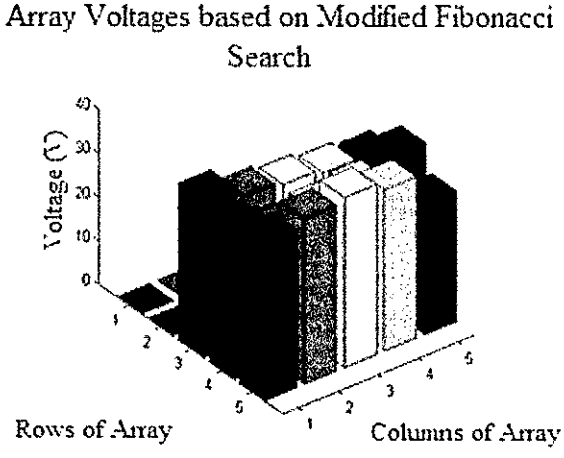

(a)

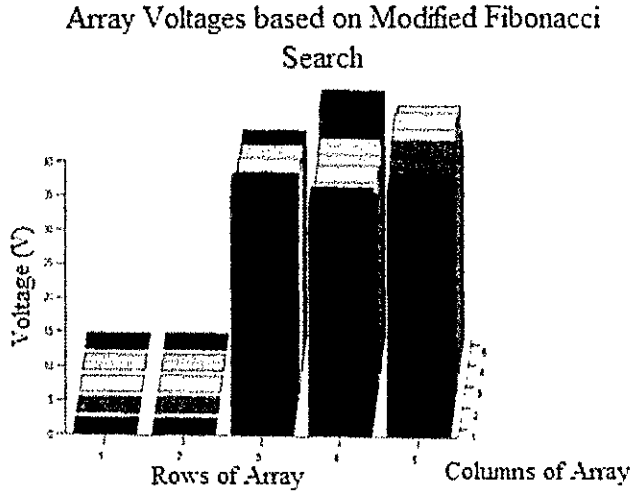

(b)

Figure 4.5. Trial 1a Full Fibonacci Array Cut Off Voltages 1(a) and 2(b).

4.2.2 Quick Search Results

In the next trial, titled Trial 1b, the Matlab code computes the MPP using the Quick Fibonacci Search Algorithm. Table 4.4 shows the data results from the Quick Fibonacci Search. Just as in the Full search, Column A represents the voltage in volts, column B represents the power in watts. The Excel row number is used to determine the iteration number by taking the row number and subtracting by one. So iteration or run two is labeled as row three in the Excel data.

Table 4.4: Trial 1b MPPT Quick Search Voltage and Power Data.

	A	B
1	Voltage(V)	Power(W)
2	11.5	19.688
3	11.1667	19.1173
4	12.5	21.3875
5	12.1667	20.8172
6	12	20.532
7	12	20.532
8	12	20.532
9	12	20.532
10	12	20.532
11	23	39.353
12	23	39.353
13	34	58.174
14	32.6667	55.8927
15	32	54.752
16	32	54.752

Table 4.4 tells us that at run 12 (row13-1) the MPP is calculated to be 58.17 watts. This is smaller than the Full Search by a difference of 7.7 watts. It is important to note that it took half the number of runs to determine the estimated MPP using the Quick Search vice the Full Search.

Figures 4.6 and 4.7 show graphs of the Quick Search MPPT, where the y axis of both graphs is the Power, and the x-axis of Figure 4.6 is the iteration number, and Figure 4.7 is the voltage respective voltage value in relation to the power.

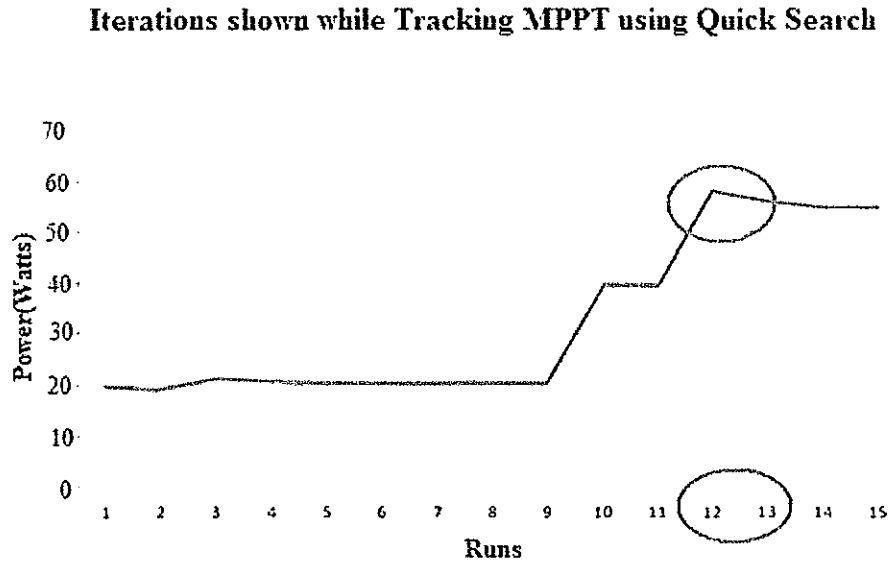

Figure 4.6: Trial 1b MPPT Iterations using Quick Search.

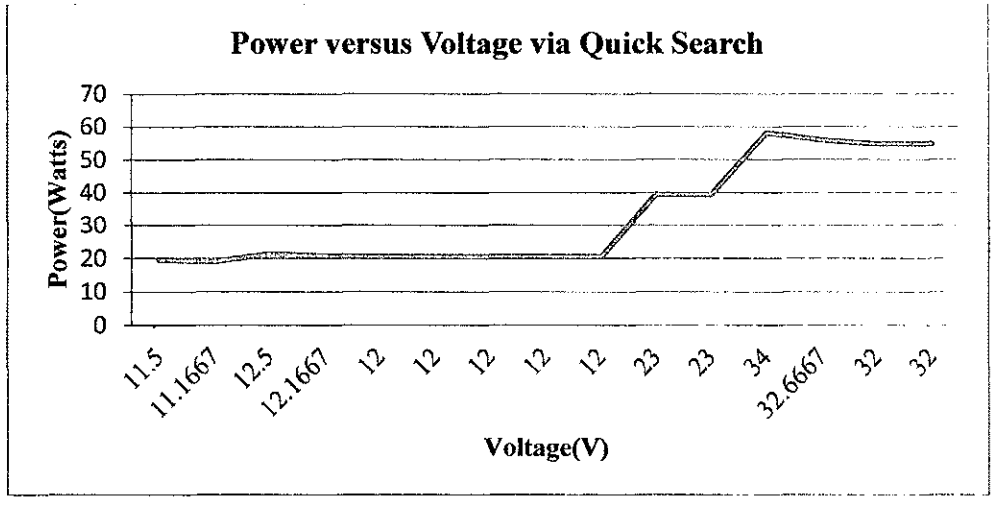

Figure 4.7: Trial 1b Power versus Voltage using Quick Search.

Since the MPP is known using the Quick Search, the code then searches the array that has PV cells outputting half the computed MPP value and turns those applicable cells off. This is depicted in Figure 4.8.

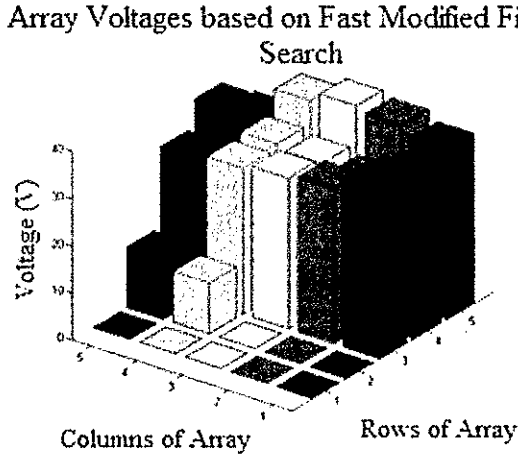

(a)

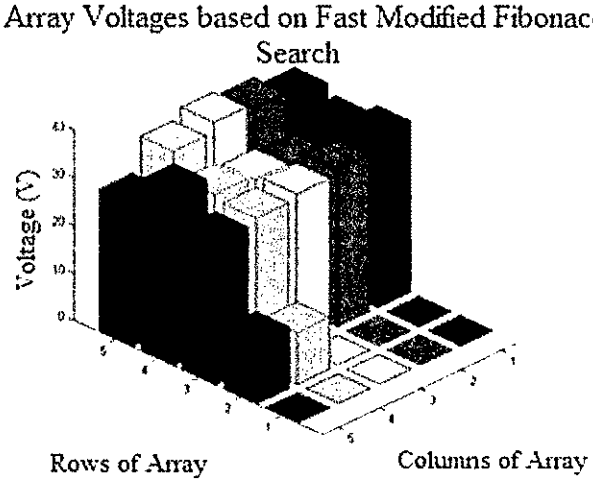

(b)

Figure 4.8: Trial 1b Quick Fibonacci Array Voltages 1(a) and 2(b).

One can note, that unlike the Full Search, the Quick search does not turn off all the PV cells that have a low power output. This is attributed to the fact, as discussed in Chapter 3, that not all the cells are searched; instead Fibonacci numbers are used to determine which element in the arrays is actually searched.

4.3 10x10 Solar Arrays Results

Next, we see how the algorithm works on larger arrays. Table 4.5 and 4.6 reveals the voltage values in volts and respective current in amperes value of each individual cells of the PV array.

Table 4.5: Trial 2 - Voltage Values of 10x10 PV Array.

Voltages(V)

11	12	13	14	12	11	13	12	11	14
10	12	14	11	10	12	11	14	12	15
11	12	14	11	13	12	14	13	12	11
42	43	42	41	43	45	42	43	45	44
44	42	41	42	46	42	41	45	47	46
46	48	49	47	46	44	45	41	48	42
46	43	42	41	43	45	42	43	45	44
44	42	41	42	46	42	41	45	47	46
45	48	49	47	46	44	45	41	48	42
47	43	42	46	48	45	43	44	45	42

Table 4.6: Trial 2 - Current Values of 10x10 PV Array.

Current

1.711	1.711	1.711	1.711	1.711	1.711	1.711	1.711	1.711	1.711
1.711	1.711	1.711	1.711	1.711	1.711	1.711	1.711	1.711	1.711
1.711	1.711	1.711	1.711	1.711	1.711	1.711	1.711	1.711	1.711
1.711	1.711	1.711	1.711	1.711	1.711	1.711	1.711	1.711	1.711
1.711	1.711	1.711	1.711	1.711	1.711	1.711	1.711	1.711	1.711
1.711	1.711	1.711	1.711	1.711	1.711	1.711	1.711	1.711	1.711
1.711	1.711	1.711	1.711	1.711	1.711	1.711	1.711	1.711	1.711
1.711	1.711	1.711	1.711	1.711	1.711	1.711	1.711	1.711	1.711
1.711	1.711	1.711	1.711	1.711	1.711	1.711	1.711	1.711	1.711
1.711	1.711	1.711	1.711	1.711	1.711	1.711	1.711	1.711	1.711

In addition, as in Section 4.2, the bar plots of the voltages is graphed and shown in Figure 4.9, where the x axis represents the row number, the y axis represents the column number and the z axis represents the voltage value in Volts.

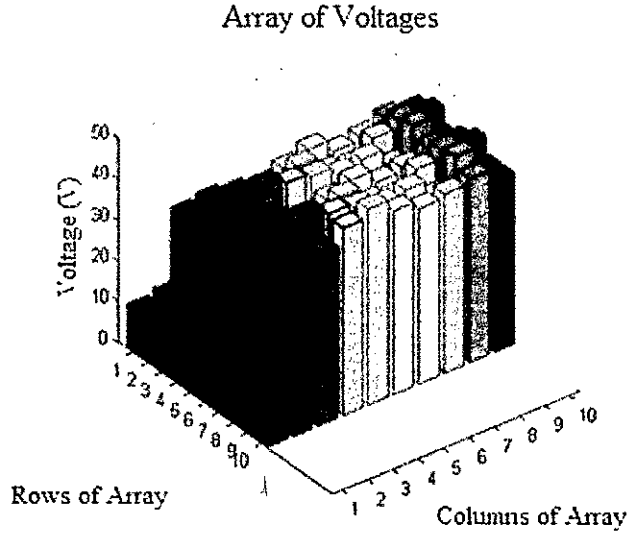

(a)

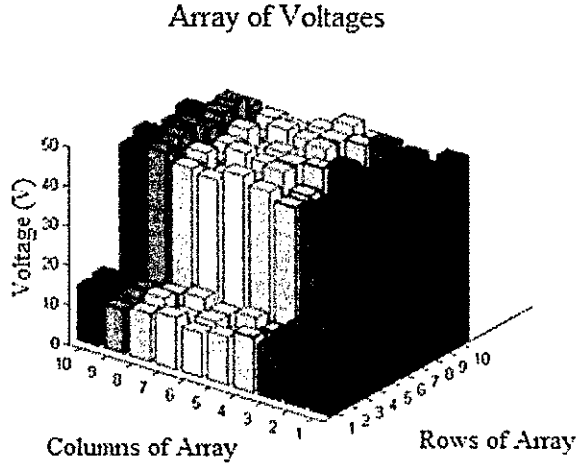

(b)

Figure 4.9: Trial 2 Bar Plots of the 10x10 PV Array 1(a) and 2(b).

4.3.1 10x10 Full Search Results

As shown in Figure 4.10, the MPP is found to be 83 Watts at the 91st run.

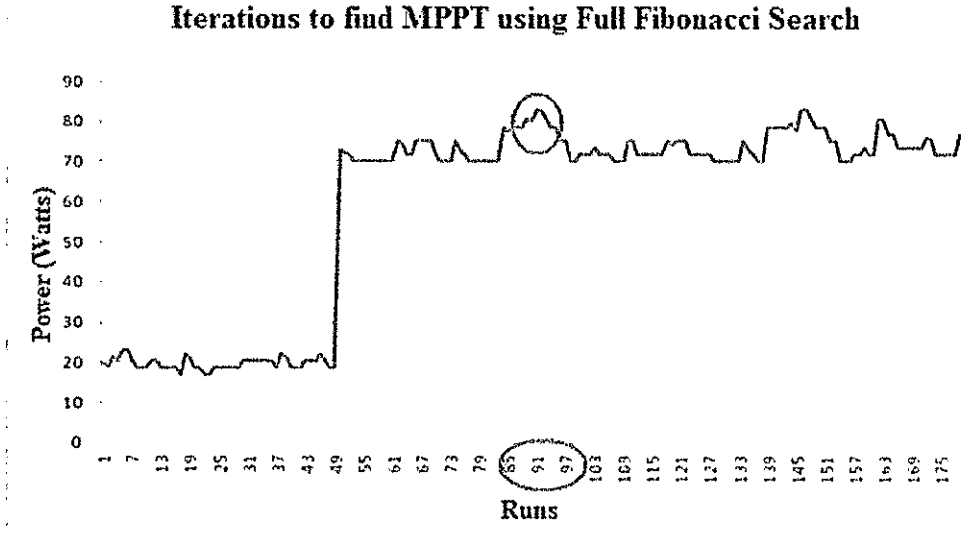

Figure 4.10: Trial 2a MPPT Iterations using Full Search.

Once the MPP was computed, the algorithm goes back to the array and searches the cells where the power output is half the MPP value. Those applicable cells are then turned off, as shown in Figure 4.11.

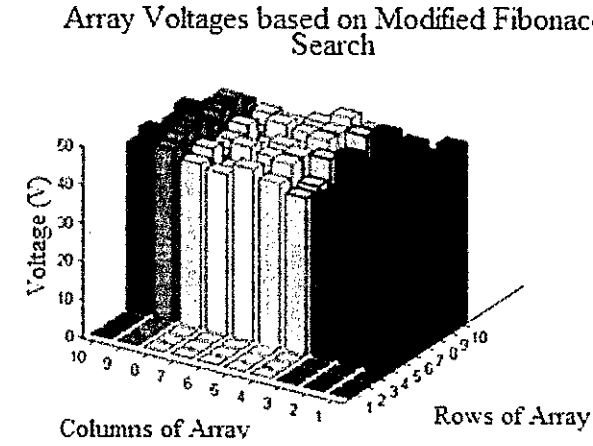

(a)

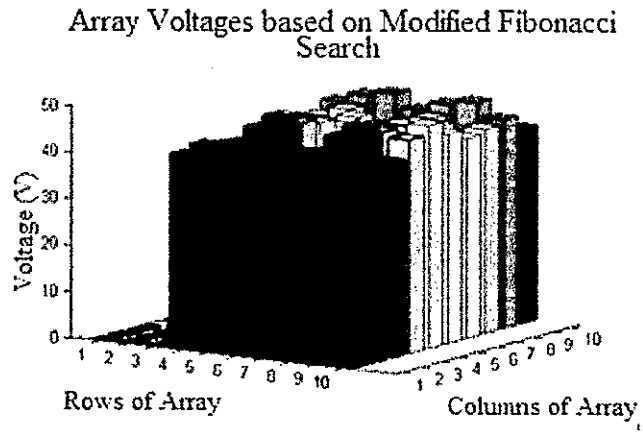

(b)

Figure 4.11: Trial 2a Full Fibonacci Array Voltages Bar Plots 1(a) and 2(b)

4.3.1 10x10 Quick Search Results

The results of the Quick Search on the 10x10 PV array shown in Tables 4.5 and 4.6 is shown in Figure 4.12 and 4.13, where the calculated MPP is 81 Watts on the 28th iteration. Next, as shown in Figure 4.13, the cells with low power output are cut off due to partial shading.

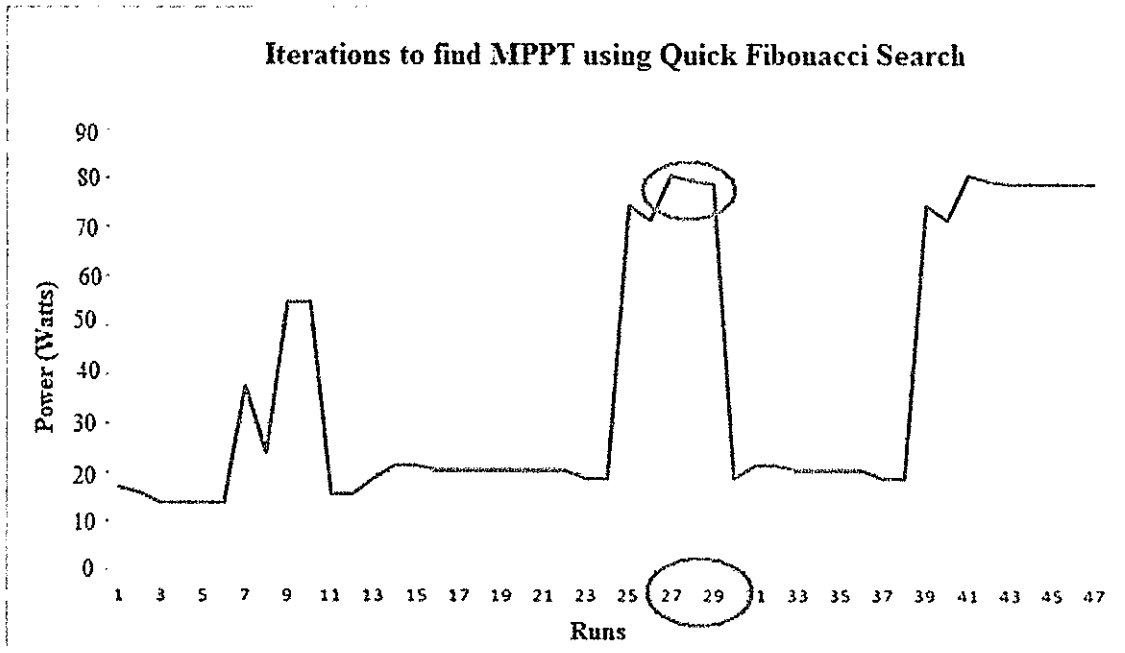

Figure 4.12: Trial 2b MPPT Iterations using Quick Search.

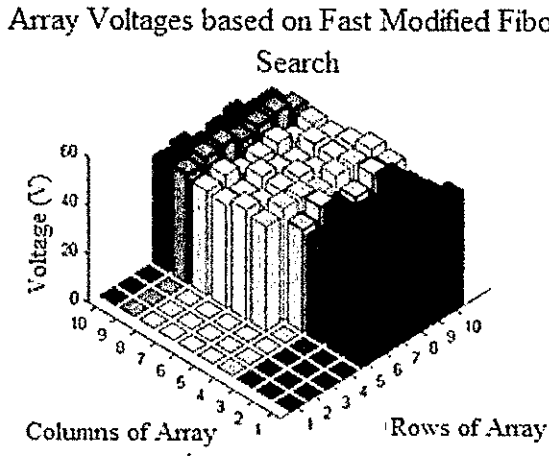

(a)

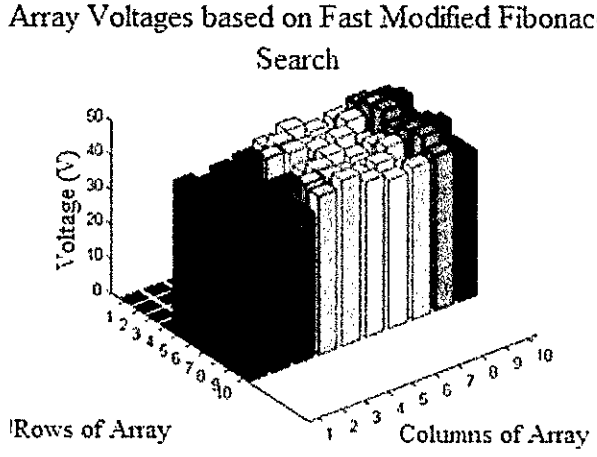

(b)

Figure 4.13.2: Trial 2b Quick Fibonacci Array Voltages 1 (a) and 2(b)

CHAPTER 5
CONCLUSIONS AND SCOPE FOR FUTURE WORK

5.1 Concluding Summary

Photovoltaic (PV) arrays of three different sizes were modeled and the performance of the two search algorithms, Fibonacci Full Search and Fibonacci Quick Search, were used to determine the maximum power point (MPP).

The two algorithms were successfully implemented and tested using the Matlab sofware. An important assumption with the array was that the given voltage and current value of each cell represents the detected value during a given moment of the daylight hours. The intent was to examine and compare the number of iterations it took to compute the MPP using the search algorithms. In return, based on the MPP value, one can, in principle, effectively turn off the PV cells that produce low power outputs, while keeping the cells that were performing at or near the MPP value turned on. The results using the two search algorithms on the 5x5 PV array and 10x10 PV arrays were plotted and observed.

5.1.1 Summary on Fibonacci Full Search Simulation Results

From the results obtained from the full search, in both the 5x5 PV array and the 10x10 PV array, the MPP was observed to be higher than the actual maximum power of the PV array. This outcome is expected because of the approximation that takes place in calculating V1 and V2 as a result of using Fibonacci numbers in the optimization computations. The number of iterations it took to determine the MPP was also noted for the 5x5 and 10x10 PV array. From the overall results it can be concluded that by using

the Full Search to determine the MPP, applicable cells can be successfully turned off that were outputting low power, within a reasonable number of iterations.

5.1.2 Summary on Fibonacci Quick Search Simulation Results

The results obtained from the Quick Search, in both the 5x5 PV array and the 10x10 PV array, the MPP was observed to be lower than the actual maximum power of the PV array and lower than the Full Search computed MPP. This arose from the fact the unlike the Full Search algorithm which searched every element in the array, the Quick Search searches selected elements in the array using Fibonacci Numbers. In addition, just as in the Full Search, the approximation that takes place in calculating and optimizing V1 and V2 are a result of using Fibonacci numbers. The number of iterations it took to determine the MPP was also noted for the 5x5 and 10x10 PV arrays. It is important to point out that the number of iterations taken to compute the MPP was significantly lower with the Quick Search than with the Full Search for both the 5x5 and 10x10 PV arrays. Since the computed MPP value is smaller than the actual power, the Quick Search is not capable of turning off all of the cells that are producing low power. From the overall results, it can be concluded that MPP using the Quick Search is not as accurate as the Full Search, nor are all of the desired PV cells outputting low power are turn off. However, the biggest advantage is the speed or number of iterations it takes to determine the MPP. Depending on whether one wishes to comprise speed with accuracy is a potential factor in determining a Quick Search versus a Full Search.

5.2 Simulations Limitations

This section will discuss several limitations of using the Fibonacci Full and Quick Search Algorithm. One limitation involves the fact that true or actual maximum power is rarely achieved. Both algorithms overestimate or underestimate the maximum power when computed. Another limitation is the corner points, or what takes place when the algorithm is at the end of a row or the last element of the array. Instead of comparing the elements below and above the cell in the array, the algorithm is limited in that it only selects the cell prior to the last element in the row. Alternatively, in the case of the last element in the column, the element before the last element in the column is collected. Despite these limitations, the overall purpose of the algorithm is to quickly give the operators working the PV system an estimate of the maximum power, the PV cells that are potentially producing high and low powers, and which cells need to be turned off to save costs, the life span of the cells, and minimize damage to the cells that are outputting low power.

5.3 Suggestions for Future Work

Issues that need to be addressed in the future for further study in this area are the limitations already discussed in Section 5.2. In addition, one could improve the algorithms by allowing the selection of not just two elements horizontally at a time for comparison, but in addition provide comparison of the elements above, below and to the left to the respective cell.

Moreover, work has only been done on small static models to represent PV systems in this thesis. Future work could use increased sizes of the arrays to much higher

numbers such as 500x5, 1000x1000 and even 5000x5000 arrays. This might be important for examining the potential effect larger PV systems may have on the search algorithms.

Other suggestive areas to investigate for future study are as listed below:

(i) Implement the models onto Simulink and tests hardware prototypes to validate and verify the performance of the system under various partial shading scenarios.

(ii) Include a dynamic, real-time algorithm for continuous monitoring and updating of the PV arrays in real time.

(iii) Investigate and compare other MPPT optimization algorithms mentioned in chapter three of this thesis. This might be important to note if the other optimization algorithms are more accurate in calculating the MPP.

REFERENCES

1. A. Belegundu, T. Chandrupatla. *Optimization Concepts and Applications in Engineering*. 2nd Edition. Cambridge, New York: Cambridge University Press, 2011, pp. 60-64.

2. A. Luque, S. Hegesdus, *Handbook of Photovoltaic Science and Engineering*, West Sussex: John Wiley & Sons, 2011, pp. 9-900,

3. A. Ubisse, A. Sebitosi, "A new topology to mitigate the effect of shading for small photovoltaic installations in rural sub-Saharan Africa," *Energy Conversion and Management*, vol. 50, no. 7, pp. 1797-1801, July 2009.

4. B. Parida, S. Inivan, R. Goic, "A review of solar photovoltaic technologies," *Renewable and Sustainable Energy Reviews*, vol. 15, no. 3, pp 1625-1636, April 2011.

5. D. Barlev, R. Vidu, R. Stroeve, "Innovation in concentrated solar power," *Solar Energy Materials & Solar Cells*, vol. 95, no. 10, pp. 2703-2725, October 2011.

6. I. Yuksel, K. Kaygusuz, "Renewable energy sources for clean and sustainable energy policies in Turkey," *Renewable and Sustainable Energy Reviews*, vol. 15, no. 8, pp 4132-4144, October 2011.

7. J. Dunlop, *Photovoltaic systems*, Orlando Parks: American Technical Publishers, inc, pp. 15-90, 2010.

8. J. Lesourd, "Solar photovoltaic systems: the economics of a renewable energy resource," *Environmental Modelling & Software*, vol. 16, no. 2, pp. 147-156, March 2001.

9. K. Williges, J. Lilliestam, A. Patt, "Making concentrated solar power competitive with coal: The costs of a European feed-in tariff," *Energy Policy*, vol. 38, no. 6, pp. 3089-3097, June 2010.

10. L. Chaar, L. Lamont, N. Zein, "Review of photovoltaic technologies," *Renewable and Sustainable Energy Reviews*, vol. 15, no. 5, pp. 2165-2175, June 2011.

11. L. Khemissi, B. Khiari, R. Andoulsi, "Low cost and high efficiency of single phase photovoltaic system based on microcontroller," *Solar Energy*, vol. 85, no. 5, pp. 1129-1141, May 2012.

12. L. Qun, X. Lu, "Matlab/Simulink-based research on maximum power point tracking of photovoltaic generation," Physics Procedia, vol. 24, pp. 10-18, 2012.

13. P. Viebahn, Y. Lechon, F. Trieb, "The potential role of concentrated solar power (CSP) in Africa and Europe - A dynamic assessment of technology development, cost development and life cycle inventories until 2050," *Energy Policy*, vol. 39, no. 8, pp. 4420-4430, August 2011.

14. R. Banos, F. Manzano-Agugliaro, F. Montoya, "Optimization methods applied to renewable and sustainable energy: A review," *Renewable and Sustainable Energy Reviews*, vol. 15, no. 4, pp. 1753-1766, May 2011.

15. R. Ramaprabhra, B. Mathur, A. Ravi, S. Aventhika. "Modified Fibonacci Search Based MPPT scheme for SPVA under partial shaded conditions." IEEE Computer Society. pp. 379-384. 2010.

16. T. Bennett, A. Zilouchian, R. Messenger, "Photovoltaic model and converter topology considerations for MMPT purposes," *Solar Energy*, vol. 86, no. 7, pp/ 2029-2040, July 2012.

17. O. Yayenie. "A note on generalized Fibonacci Sequences." Applied Mathematics and Computation. vol. 217, pp. 5603-5611, 2011.

18. V. Salas, E. Olias, A. Barrado, A. Lazaro. "Review of the maximum power point tracking algorithms for stand-alone photovoltaic systems." Solar Energy Materials & Solar Cells Vol 90, p 1555-1578, 2006.

19. "Types of renewable energy." Internet: http://www.renewableenergyworld.com/rea/tech/home, [August 2012].

20. "Wind Power." Internet: http://en.wikipedia.org/wiki/Wind_power [August 2012].

21. "What Causes Wind." Internet: http://www.weatherquestions.com/What_causes_wind.htm, November 26, 2010[August 2012].

22. "Hydropower." Internet: http://en.wikipedia.org/wiki/Hydropower [July 2012].

23. "Geothermal Energy." Internet: http://www.renewableenergyworld.com/rea/tech/geothermal-energy [August 2012].

24. "Geothermal Energy." Internet: http://en.wikipedia.org/wiki/Geothermal_energy [July 2012].

25. "Solar Energy." Internet: http://en.wikipedia.org/wiki/Solar_energy [July 2012].

26. "Solar Power." Internet: http://en.wikipedia.org/wiki/Solar_power [August 2012].

VITA

Felicia Tyyan Farrow,
Department of Electrical and Computer Engineering
Old Dominion University, Norfolk VA 23529
Email: ffarr004@odu.edu

Academics:
BS in Electrical Engineering from Old Dominion University, (May 2009, GPA 3.71)

Research Experience:
Bioelectric Research Center – Student Research Assistant (November 2008-May 2009)

- Aid professors, researchers, and graduate students in bioelectric research
- Designed, simulated, tested Blumeline Generator Model and compared models with actual lab designs

Old Dominion University- Department of Electrical/Computer Engineering: Research Electromagnetic Interference (January 2008-March 2009)

- Use PSPICE/MATLAB simulators to model interfering signals on avionic circuits
- Impose interfering signals on different sample circuits and observe results

Old Dominion University – Undergraduate Research Program (USRP) Jefferson Laboratory- Center For Advanced Studies of Accelerators (September 2007- December 2007)

- Studied Beam Position Monitors and Beam Current Monitors
- Studied Radio Frequency Modules

Professional Experience:
Commander Operational Test and Evaluation Force- Navy Acquisition Intern / Electrical Engineer Fall 2010 – Present

- Core Team Facilitator for Mission Based Test Design Process
- Assist and Support Design of Experiment Testing Design
- Test Planning Division

Office of Naval Research -Navy Acquisition Intern, Summer 2012

- Draft Technology Roadmap for Autonomous Vehicle Program

VX-1 Air Test and Evaluation Squadron, Summer 2011

- Collected Data and Supported Air Squadron with Mine Countermeasures Testing

Planit Technology Group, LLC – Software Assistant Support (Intern) Summer 2009

- Consultant at Amerigroup's Application Management Department

Science Application International Corporation (SAIC) -Intern (June-October 2008)

- Involved in Renewable Energy Solutions; Offshore Wind, Wave, Tidal, and Biodiesel
- Assisted supervisor in writing reports, and presentations.
- Studied and wrote a report on the advantages and disadvantages of high voltage direct current cables (HVDC) and high voltage alternating current cables (HVAC) for underwater power transmission.

NASA Summer High School Apprenticeship Research Program, NASA SHARP Summer Intern (June 2004- August 2004)

- Langley Research Center, Electromagnetic Research Laboratory
- Conducted Research in the electromagnetic branc